https://doi.org/10.5194/egusphere-2024-4175
Preprint. Discussion started: 27 January 2025

Characterization of Northwest African coastal Upwelling Systems

Dametoti Yamoula[1,2], Ifeoluwa A. Balogun[1,2], Bamol A. Sow[3]

[1]Department of Meteorology and Climate Science, Federal University of Technology, Akure, Nigeria
[2]West African Science Service Centre for Climate and Adapted Land Use, Federal University of Technology, Akure, Nigeria
[3]Laboratoire d'Océanographie, des Sciences de l'Environnement et du Climat (LOSEC), Université Assane Seck de Ziguinchor (UASZ), Senegal

Correspondence to: Dametoti Yamoula (yamolua.d@edu.wascal.org)

Abstract. Coastal upwellings are critical for nutrient supply, biological productivity, socio-economic activities, local weather patterns and regional climate variability. This study investigated characteristics of the Northwest African coastal upwelling system, including the Senegal-Mauritania and Gulf of Guinea coastal upwelling regions. The spatial and temporal variability were analysed using physical and biogeochemical ocean variables from 1982 to 2022. The analysis focused on upwelling indices derived from sea surface temperatures (SSTs), wind stress and chlorophyll-a concentration during the boreal winter-spring and summer, when upwelling peaks in the Senegal-Mauritania and Gulf of Guinea upwelling systems, respectively. Additional indicators such as the annual cycles of sea level anomaly, ocean surface current velocity, geostrophic balance, salinity, nitrate and dissolved oxygen in surface waters were also examined as upwelling indicators. Upwelling trends were investigated by comparing the results of different datasets. Results highlight the complex interplay of local and large-scale processes that influence the dynamics of coastal upwelling in Northwest Africa. The variability in these coastal upwelling regions was not only influenced by local and remote wind forcing, but also by large-scale climatic drivers such as El Niño Southern Oscillations (ENSO) and Atlantic Niño events. These climatic factors influence the intensity and frequency and duration of upwelling seasons. In the Senegal-Mauritania coastal upwelling, a strong relationship was observed between upwelling and the equatorial ENSO events from late winter to the early spring, with a notable reduction of upwelling intensity after the peak of El Niño in the equatorial Pacific. In the Gulf of Guinea, the summer upwelling intensity was affected by the equatorial Atlantic mode and often decoupled from local wind forcing, providing new insights into alternative upwelling drivers.

Keys words: Annual cycle of upwelling, cumulative upwelling index, Northwest African coastal upwelling systems.

1 Introduction

Coastal upwelling is notable for its high biological productivity, vital local fisheries and significant socio-economic impacts on neighbouring countries (Koné et al., 2017; Amemou et al., 2020). It is traditionally defined as a process by which nutrient-rich cold water rises onto the continental shelf, compensating for the seaward drift of surface water under the combined action of upwelling-favourable wind stress and the Earth's rotation (Ekman, 1905). Bakun (1973, 1975), expanded this by

https://doi.org/10.5194/egusphere-2024-4175
Preprint. Discussion started: 27 January 2025

emphasizing on the influence of seasonal and geographical variations in coastal upwelling. He highlighted that the strength and extent of upwelling can vary based on wind patterns, topography, and other environmental factors. The natural variability of coastal upwellings located along the eastern boundaries of ocean basins (such as Humboldt, California, Benguela and Canary upwelling systems) has been associated to the local weather patterns and large-scale climate drivers, including ENSO, North Atlantic Oscillations (NAO), Southern Oscillation Index (SOI) and Pacific Decade Oscillations (PDO) events (Bograd et al., 2009; Yu et al., 2020). While the local variability of upwelling is partly driven by natural processes, their intensity, frequency and duration are strongly affected by global warming, primarily due to the anthropogenic rise in atmospheric CO2 and the resulting alterations in weather and climate patterns (Gruber et al., 2011).

In this study, we review the current characteristics of the Northwest African coastal upwelling system, including the Senegal-Mauritania and Gulf of Guinea coastal upwelling regions. These features are indicators of the recent spatial and temporal variability of coastal upwelling off West Africa, and are needed to predict future variability. In the literature, the drivers and impacts of both coastal upwelling systems are well documented. In the Senegal-Mauritania coastal upwelling system (SMUS), the variability of coastal upwelling is mainly attributed to the trade winds modulated by Azores subtropical high-pressure (Ndoye et al., 2014; Faye et al., 2015; Sylla et al., 2019), and the position of the Intertropical Convergence Zone (ITCZ) (Pelegri et al., 2006; Valdes & Deniz-Gonzalez, 2015). Ekman theories are generally used to describe this upwelling system (Benazouzz et al., 2014; Sylla et al., 2019). Using the regional ocean models, Ndoye et al., (2014, 2017) have showed additional factors such coastal geometry and mesoscale eddies which affect the upwelling intensification. The temporal and spatial variability of upwelling have been described with upwelling indices based on SST anomalies, wind stress patterns and chlorophyll-a concentration (Demarcq and Faure, 2000; Caniaux et al., 2011; Cropper et al. 2014, Benazouzz et al. 2014). These different upwelling indices have allowed to determine metrics and changes in coastal upwelling intensity.

The variability of the coastal upwelling observed along the Gulf of Guinea coast, especially between 10°W and 5°E (Caniaux et al. 2011), has been attributed to several biophysical processes, including the local zonal wind stress, equatorial dynamics (Clarke, 1983; Philander et al., 1990; Picaut, 1983), such as the eastern propagation of Kelvin and coastal trapped waves (Philander and Pacanowski, 1981) and ocean currents (Djakouré et al. 2017). In Gulf of Guinea coastal upwelling system (GGUS) as in many tropical regions, peaks of wind stress and ecosystem productivity are not aligned (Körner et al., 2024). Detailed studies have shown that wind stress alone cannot explain upwelling processes in these regions. Therefore, other physical mechanisms beyond offshore Ekman transport, such as equatorial currents, surface heat fluxes, remote forcing via equatorial waveguides (Weisberg et al., 1979; Philander, 1979; Hormann and Brandt, 2009), vertical mixing (Brandt et al., 2023), mesoscale eddies (Djakuré et al. 2014) and large-scale climate drivers (Bograd et al., 2009; Yu et al., 2020) have been explored to understand upwelling processes in these regions. Recent findings from high-resolution tropical Atlantic Ocean model experiments (Illig et al., 2024) highlight that coastal variability is influenced by both equatorially forced coastal-trapped waves and reflected equatorial Rossby waves. Polo et al., (2008) further revealed recurrent and continuous poleward propagations of coastally trapped Kelvin waves over thousands of kilometres, extending as far as 10°–15° latitude along the West African coastline. Using sea surface height (SSH) correlations, they quantified the phase speed and underscored the

https://doi.org/10.5194/egusphere-2024-4175
Preprint. Discussion started: 27 January 2025

65 importance of remote forcing, showing clear evidence of intra-seasonal Kelvin waves' influence on coastal upwelling regions during boreal autumn–winter. Some studies suggested a minimal direct influence of equatorial Kelvin waves on boreal summer SST variability (Hormann and Brandt, 2009) and emphasized on the role of local wind variability and vertical transport. Using the regional ocean model, Djakouré et al., (2014) showed that mesoscale eddies cannot be considered as the driving force behind coastal upwelling in the Gulf of Guinea despite the role they play in upwelling intensification, and highlighted the
70 Guinea Current (Djakouré et al. 2017). Recently, Alory et al., (2021) found that the Niger River plume acts as a barrier limiting the intensification of the eastern edge of the Guinean Gulf coastal upwelling.

Since 1990, Andrew Bakun suggested that increasing greenhouse gas concentrations due to climate change could intensify upwelling-promoting winds in the eastern boundary current systems (EBUSs). This Bakun's hypothesis was partially validated,
75 especially in upwelling regions located at high latitudes (Seydman et al., 2014). Using historical observations (Benazzouz et al., 2015) and under climate change scenarios RCP8.5 (Sylla et al., 2019, Varela et al., 2021), previous studies have found a northward displacement of upwelling with a moderate increase trend of upwelling-favourable winds in the Canary upwelling system. But they underlined that Bakun's hypothesis does not hold in the SMUS (10°-21°N), where upwelling indices are nearly constant. However, Bakun's mechanism has suffered a setback in recent studies where authors found changes in
80 upwelling independently to wind stress forcing (Chang et al., 2023) and anthropogenic climate change (Abrahams et al., 2021). This reopening the question of the impact of climate change on Northwest coastal upwelling systems. Studies have shown that the Northwest African coastal upwelling influence regional precipitations (Brandt et al., 2011; Fontaine & Janicot, 1992; Lamb, 1978; Rodríguez-Fonseca et al., 2015), as well as primary production, pelagic fish habitat, and marine resource abundance (Binet & Marchal, 1993). They largely inflect the onset and amplitude of the African monsoon (Brandt et al., 2011; de
85 Coëtlogon et al., 2023). However, the predictability of Northwest African upwelling cells remains a topic of active debate, particularly regarding the roles of remote forcing and the propagation of Kelvin waves in the eastern Atlantic (Polo et al., 2008; Illig et al., 2024). Although drivers and impacts of this coastal upwelling are well documented, changes in intensity and frequency remain challenges. This study aims to investigate on the recent characteristics of both SMUS and GGUS located in between 10º-25ºN and 4º-7ºN, respectively. In the second section, we present data and methods used for this study. The third
90 section presents and discusses results on different characteristics of each upwelling region before concluding this study.

2 Materials and methods

2.1 Data

Different physical and biogeochemical marine variables from several sources are used in this study. The reanalysis data include Ocean Reanalysis System 5 (ORAS5, Zuo et al., 2018) and the fifth-generation atmospheric reanalysis (ERA5, Hersbach et
95 al., 2020) provides by the European Centre for Medium-Range Weather Forecasts (ECMWF), and the global Mercator Ocean reanalysis (GLORYS) product (Lellouche et al., 2021). The observation products are constituted of Hadley Centre Sea Ice and

https://doi.org/10.5194/egusphere-2024-4175
Preprint. Discussion started: 27 January 2025

SST dataset version 1 (HadISST1; Rayner et al. 2003) and the continuous satellite observations of SST (OSTIA, Good et al., 2020). ORAS5 and HadISST products are monthly time-scale while ERA5, GLORYS and OSTIA are daily. Additionally, climate indices such as Niño 3.4 and NAO were obtained from National Oceanography and Atmospheric Administration Climate Prediction Center (NOAA-CPC) (see data availability). The bathymetry data were collected from the General Bathymetric Chart of the Oceans (GEBCO). All the data were remapped onto 0.25º grid by bilinear interpolation and used to analyze the annual cycle, interannual variability and trends of coastal upwelling in each region. The characteristics of data are summarized in the following table (Table) including type of dataset, variables used, resolution and period covered.

Table: Different datasets and resolution used in this study

Dataset	Types	Variables	Resolution	Cover period
ORAS5	Ocean reanalysis	SST, sea surface salinity, zonal and meridional wind stress, zonal and meridional velocity	0.25ºx0.25º	1980 - 2023
ERA5	Atmospheric reanalysis	SST, zonal and meridional wind components	0.25ºx0.25º	1980 - 2023
HadISST	Station observations	SST	1º x 1º	1980 - 2023
OSTIA	Satellite	SST	0.05ºx0.05º	1982 - 2022
Global Ocean reanalysis (GLORYS)	Ocean reanalysis	SST, zonal and meridional wind stress, zonal and meridional velocity, sea water salinity, sea level anomaly	0.083ºx0.083º	1993-2020
		Oxygen (o2), nitrate (No3)	0.083ºx0.083º	2020-2021
NOAA	Satellite	Chlorophyll-a concentration	0.05ºx0.05º	1997-2023
NASA	Climate indices	Niño 3.4 and NAO	Time-series	1982-2023

The reasonable agreement between satellites and reanalyses products have increased our confidence in the ability of both data to reproduce the annual cycle of upwelling.

2.2 Methodology

Upwelling indices (UI) are used in numerous studies (Demarcq and Faure, 2000; Caniaux et al., 2011; Cropper et al., 2014; Benazouzz et al., 2014; Bordbar et al., 2021) as powerful tools to analyze coastal upwelling dynamics. In this study upwelling indices based on wind stress (Ekman suctions), SST, chlorophyll-a concentration and sea level anomaly were used to characterize the annual cycle and interannual variability of upwelling in both Senegal-Mauritania and Gulf of Guinea coastal upwelling systems.

https://doi.org/10.5194/egusphere-2024-4175
Preprint. Discussion started: 27 January 2025

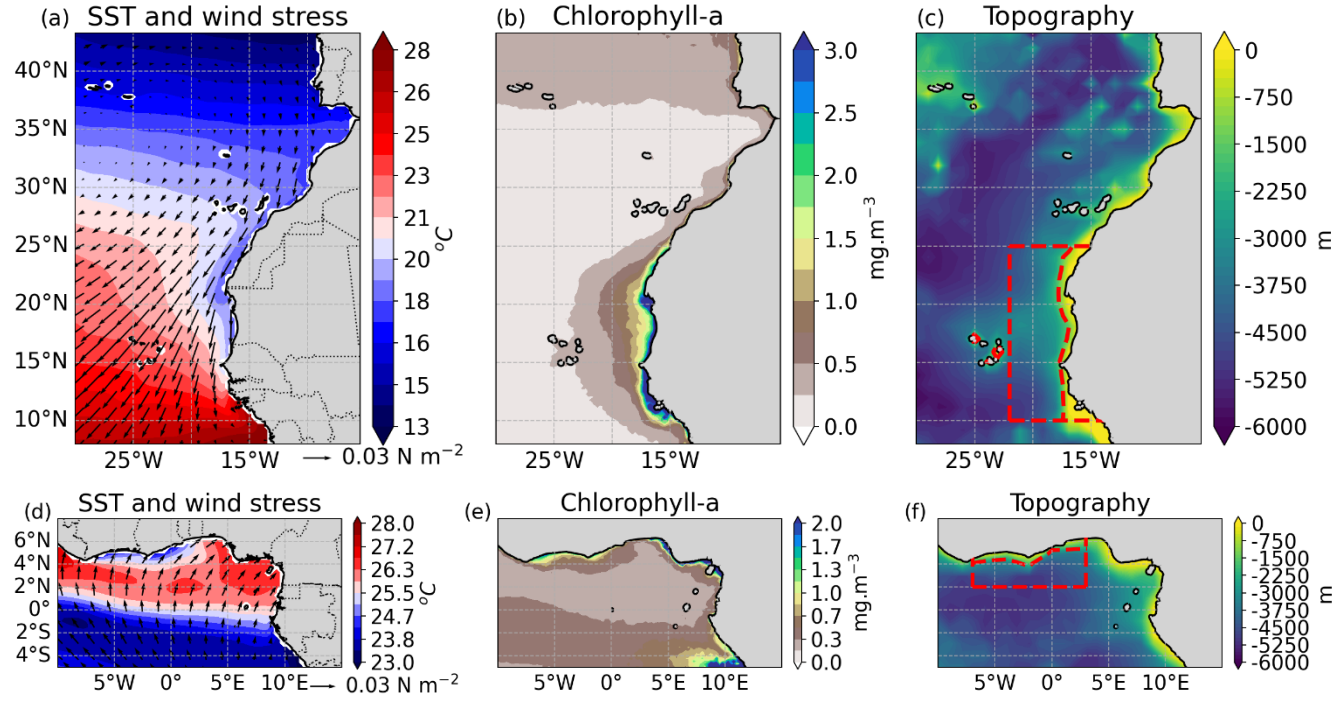

Figure 1: (a), (d) Mean sea surface temperature SST (colours) and wind stress fields (arrows) during winter-spring (December-May) and summer (July-September) in the Senegal-Mauritania and Gulf of Guinea upwelling systems, respectively. (b), (e) Chlorophyll-a concentration. (c), (f) Topography. Red dash lines show the extent of the coastal and offshore boxes. The coastal box was defined using the 1500 m and 2000 m isobath including the continental shelf and slope. The offshore box was from 5° and 2° to the coast in both upwelling regions, respectively.

As coastal upwelling occurs on the continental shelf, we have firstly defined the coastal and offshore boxes using the General Bathymetric Chart of the Oceans (GEBECO) bathymetry (Fig. 1c). The coastal boxes were defined using the 1500 m and 2000m isobaths (Fig. 1c, f), including the continental slope, respectively in the SMUS and GGUS. This region corresponds also the lower SST (Fig. 1a, d) and maximum concentration of chlorophyll-a (Fig. 1b, e) areas. The offshore boxes extend form 5° and 2° far away to the coast (Cropper et al., 2014; Sylla et al., 2019; Bordbar et al., 2021). Wind stress fields and SST were extracted in the two boxes for computing UI. However, the limited extent of the continental shelf and slope, with its steep slopes to the east of the Gulf of Guinea (Togo-Benin), could have an impact on the productivity of coastal ecosystems.

According to Ekman's (1905) theory of wind-induced ocean circulation, ocean surface waters with a homogeneous density structure, subjected to a persistent surface wind, undergo a regular motion governed by an equilibrium between the Coriolis

https://doi.org/10.5194/egusphere-2024-4175
Preprint. Discussion started: 27 January 2025

force and wind-induced frictional force. Strong winds blowing parallel to the coast create a divergence of surface waters and cause alongshore transport (Ekman transport) within the Ekman layer. This movement results in the replacement of the surface water by nutrient-rich cold waters that are brought up through upwelling. This process can lead to notable SST differences between coastal areas and the open ocean. Based on Ekman theory, the zonal (M_x) and meridional (M_y) Ekman transports were computed in each upwelling region using the following equations:

$$M_{(x)} = \frac{\tau^y}{\rho_w . f}\ , \qquad M_{(y)} = -\frac{\tau^x}{\rho_w . f}\ where\ f = 2\Omega.\sin(\varphi) \tag{1}$$

- τ^x and τ^y are zonal and meridional wind stress components;
- $\rho_{w=}1025\ Kg.m^3$ is sea water density; f is the Coriolis parameter;
- $\Omega = 7.14 * 10^{-5}\ s^{-1}$ is the momentum of the earth rotation; and φ is the latitude

The contribution of wind stress curl was also analyzed. Regardless of the presence or not of a coast, any spatially heterogeneous wind causes to a divergence or convergence of Ekman transport which leads to vertical upwelling or downwelling water respectively. This type of downwelling (negative value) or upwelling (positive value) is called Ekman pumping (W_e) or wind stress curl driven (WSCD) upwelling or downwelling and is obtained by:

$$W_e = \frac{1}{\rho_w . f}\left(\frac{\partial \tau^y}{\partial x} - \frac{\partial \tau^x}{\partial y}\right), \text{Where } \frac{\partial \tau^y}{\partial x} - \frac{\partial \tau^x}{\partial y} \text{ is the wind stress curl} \tag{2}$$

The total wind-driven upwelling index was obtained by adding the upwelling index drained by the local wind and that drained by alongshore wind. Before computing these two upwelling indices, we derived the wind stress components from the ERA5 near-surface 10 meters wind components by following this bulk formula:

$$\tau^{(x)} = \rho_a * C_d * |w_s|u_{10};\ \ \tau^{(y)} = \rho_a * C_d * |w_s|v_{10},\quad where\ ws = \sqrt{({u_{10}}^2 + {v_{10}}^2)} \tag{3}$$

Where:

- ρ_a = 1.22 kg m^{-3} is the air density, C_d = 0.0013 is the drag coefficient,
- w_s, u_{10}, v_{10} are wind speed, zonal and meridional wind components, respectively.

The SST response during upwelling period was examined. Upwelling index based on SST gradient (∇SST) was calculated between coastal upwelled-water (SST_{in}) and offshore (SST_{off}) boxes. The spatial extension of coastal upwelling was localised under 25°C (Caniaux et al., (2011). The SST gradient was computed as:

$$\nabla SST = SST_{off} - SST_{in} \tag{4}$$

https://doi.org/10.5194/egusphere-2024-4175
Preprint. Discussion started: 27 January 2025

Annual cycles of sea level anomaly and ocean surface current velocity over the coastal region were used to analyse the influence of remote forcing due to equatorial dynamics (Kelvin and coastal trapped waves) and global ocean circulation. The effects of the onshore geostrophic transport (T_g) have been estimated using sea surface height (SSH) over the ocean mixing layer depth (MLD) (Sylla et al., 2019).

$$T_g = MLD \times \frac{g}{f}(SSH_{al} - SSH_{on}) \quad (5)$$

where T_g is the vertical transport due to the SSH gradient in the mean of MLD (in meters); g is the gravity coefficient (g = 9.81 m s^{-2}), $SSH_{al} - SSH_{on}$ is the difference between alongshore and onshore SSH at the horizontal direction. In the SMUS, T_g was estimated of the zonally averaged geostrophic transport, while in the GGUS, it was estimated of the meridionally averaged geostrophic transport. T_g is counted negative eastward following the sign convention used to quantify the upwelling. The annual cycles of sea surface salinity, chlorophyll a concentration, oxygen and nitrate nutrients were used as additional indicators to characterize the biogeochemical productivity of upwelling systems.

The cumulative upwelling index (CUI) was used to analyse the interannual variation of coastal upwelling in both SMUS and GGUS. The daily Ekman transport and the SST gradient were integrated separately over the years at four sections within the SMUS (from 10°-25°N), and two sections within the GGUS (7°W-4°E) separated by 4° latitude. The results allowed to estimate the climatological start transition index (STI, start date), maximum magnitude, end date and length of the upwelling season; and to identify extreme upwelling years. Before integrating the upwelling index, the month with maximum downwelling was determined. The STI was defined as the date when the minimum CUI value was reached, marking the beginning of a sustained positive upwelling index. The end of upwelling (END) was defined as the date when the CUI reached its maximum value, after which downwelling prevailed. In the SMUS, the upwelling STI was calculated between August and next January. In the GGUS the STI was computed between January to July. The integrated CUI also allowed the identification of individual years with extreme upwelling events. Additional upwelling metrics as the length of upwelling season (i.e., duration between STI and END) and the total upwelling magnitude (TUM) (i.e., total integrated CUI between STI and END) were estimated the in each region. The TUM is obtained by:

$$TUM = \sum_{STI}^{END} CUI(t) \quad (6)$$

For the comparative analysis, these upwelling indices were computed using reanalyzes and observations (see data). Long-term trends in upwelling indices were analysed using linear regression models based on the gradient descent fit. In addition, the Pettitt statistical test was used to detect changes in upwelling indices in both upwelling regions. Composite and correlations

https://doi.org/10.5194/egusphere-2024-4175
Preprint. Discussion started: 27 January 2025

analyses for ten equatorial Pacific ENSO ten equatorial Atlantic mode of variability were used to analyse the connectivity of coastal upwelling to the Equatorial ENSO and Atlantic Niño. The equatorial Pacific ENSO area was defined between 170W-90W and 5N-5S from the Equator. The equatorial Atlantic mode was located between 20N-0 and 3S-3N (Nnamchi et al., 2021). The ENSO mode includes five extremes El Nino (1983, 1992, 1998, 2010 and 2016) and five extremes La Nina (1985, 1989, 2000, 2008 and 2011) events. The equatorial Atlantic mode includes five extremes warming (1988, 1995, 1999, 2009 and 2020) and five extremes cooling (1982, 1983, 1997, 2004 and 2012) events. These events were detected analysis the SST anomalies.

3 Results

3.1 Annual cycle of Northwest African coastal Upwelling Systems

This section analyses the seasonality of upwelling over the Senegal-Mauritania and Gulf of Guinea coasts. Upwelling indices, such as SST gradient, Ekman transport, chlorophyll-a concentration and other additional indicators were used to examine upwelling metrics such as timing (onset and end dates), intensity and duration in each upwelling region.

3.1.1 Senegal-Mauritania Upwelling System (SMUS)

In the SMUS, the annual upwelling cycle was derived from the zonal Ekman transport (Fig. 2) and the SST gradient (Fig. 3). The two upwelling indices show a permanent upwelling between 21°-25°N and a seasonal upwelling (from December to May) between 10°-21°N. The cumulative upwelling index calculated by integrating the zonal Ekman transport, indicates that the seasonal upwelling starts on the 120th day after the maximum downwelling observed in August, and extends over 245 to 270 days. The maximum intensity of the upwelling was observed in April (152 days after the onset date), while the minimum peak of the upwelling coincides with the maximum downwelling in August (Fig. 2).

https://doi.org/10.5194/egusphere-2024-4175
Preprint. Discussion started: 27 January 2025

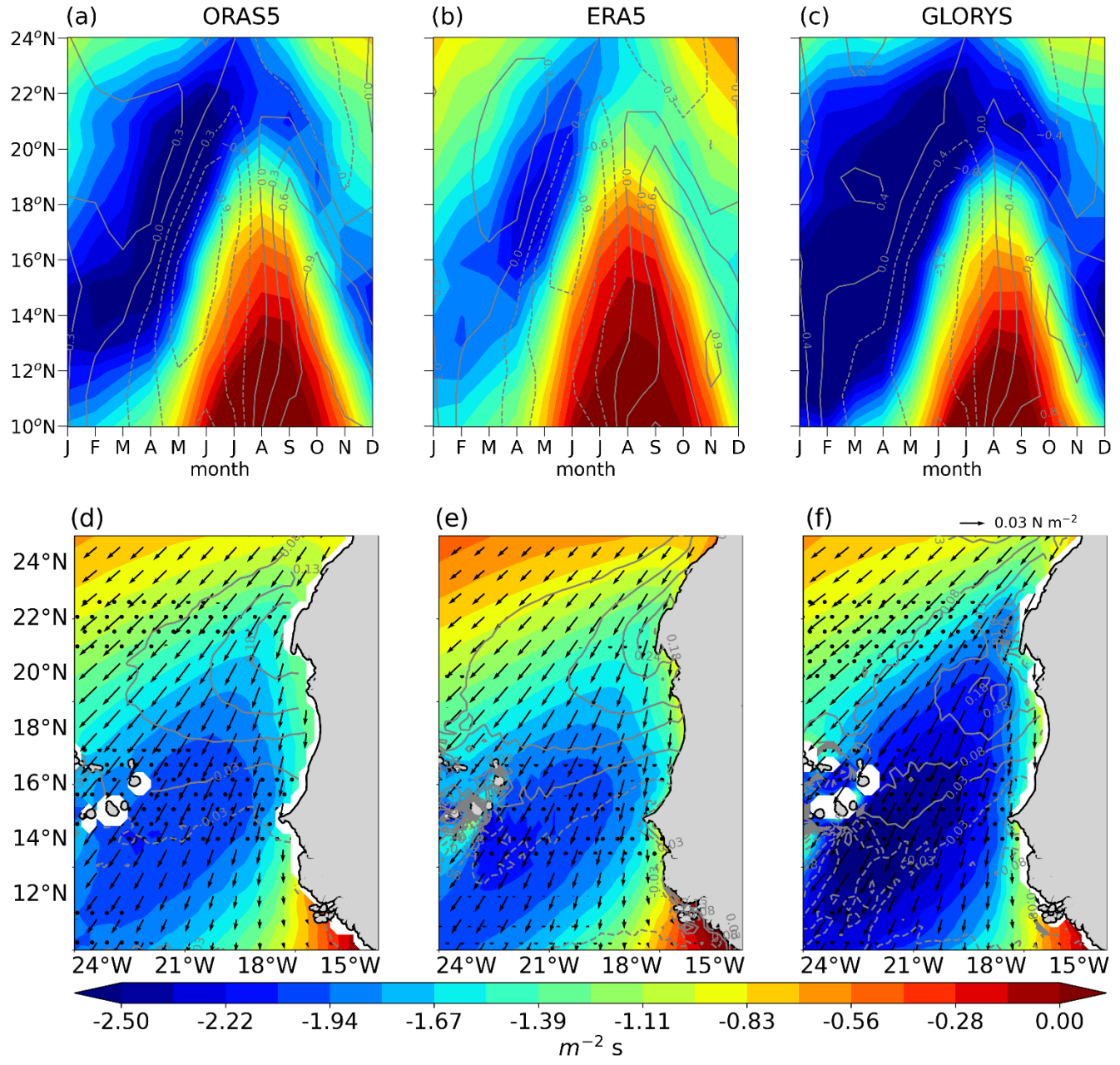

Figure 2: Wind driven-upwelling in the SMUS derived from ORAS5, ERA5 and GLORYS wind stress fields: a-c Annual cycle of zonal Ekman transport (colours) and wind stress curl driven upwelling indices (contours). d-f show winter and spring (from December to May: DJFMAM) mean states of wind stress (arrows), zonal Ekman transport (colours) and wind stress driven upwelling (contours). Black dots represent the correlation coefficient (r>0.5) between zonal Ekman transport and zonal SST gradient. Negative values of Ekman transport and positive values of wind stress curl-driven show upwelling, while the opposite values indicate downwelling.

https://doi.org/10.5194/egusphere-2024-4175
Preprint. Discussion started: 27 January 2025

This result reflects the dominant role of the Ekman transport. Similar characteristics of upwelling were observed with the zonal SST gradient (Fig. 3), but with a one month lag between the peaks of wind-driven upwelling and the SST response. The maximum peak of the coastal SST gradient is observed in March, one month before the peak of the Ekman transport. This shows the strong relationship between the zonal Ekman transport driven by the meridional wind stress and the coastal SST gradient. The linear correlation analysis between zonal Ekman transport and SST gradient at each grid point shows a strong coherence in some regions near the coast (>0.5). This good agreement between zonal Ekman transport and SST gradient reflects the fundamental role of coastal Ekman drifts. However, the correlation coefficient is statistically weak in the south (10º-13ºN), where the highest SST was observed. This highest SST drive the weakening of the surface wind stress patterns.

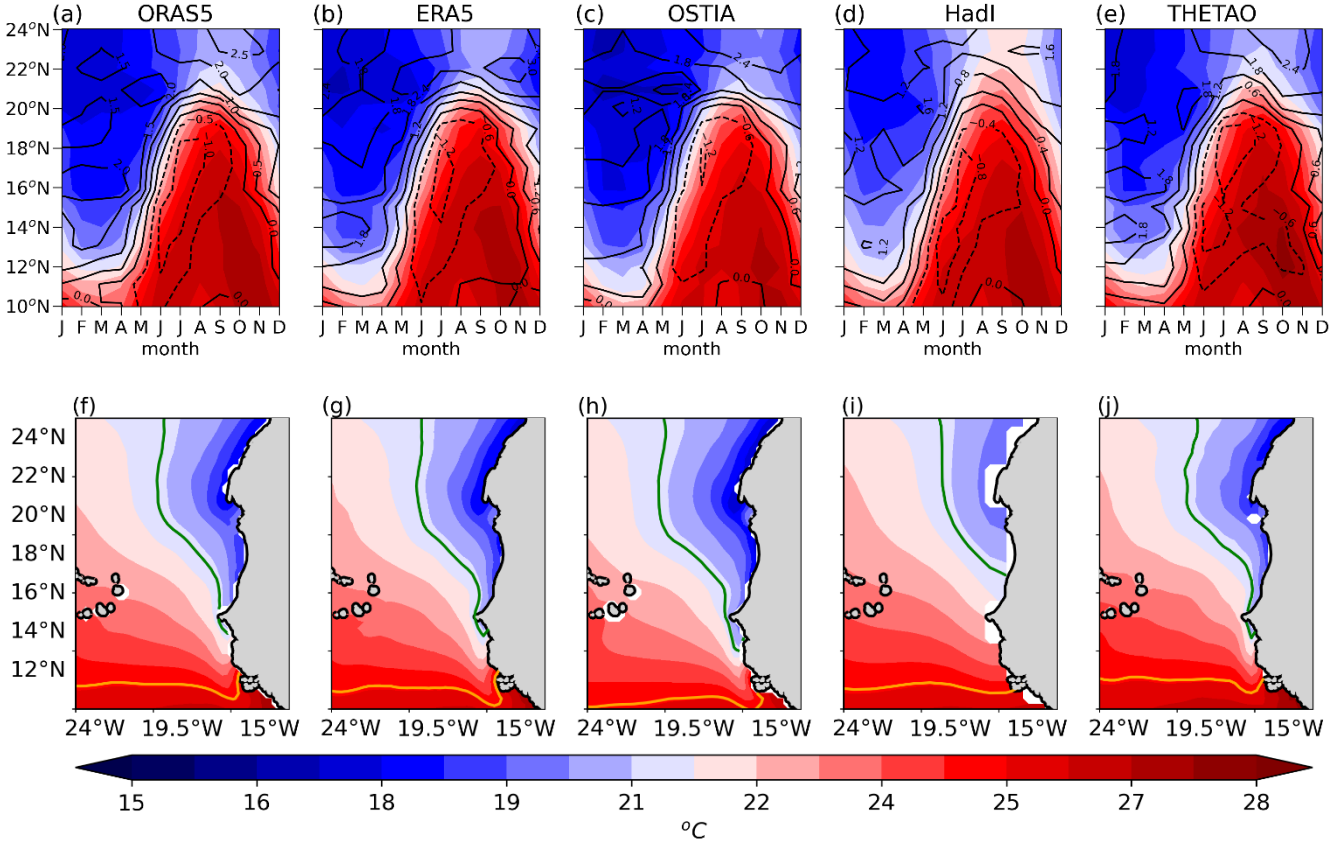

Figure 3: Seasonal variability of SST patterns in the SMUS derived from ORAS5, ERA5, OSTIA, HadISST and GLORYS (Thetao) datasets: a-e Annual cycle of SST (colours) and upwelling indices (contours) in the SMUS. f-j SST mean states during upwelling season from December to May (colours). Green lines show the minimum SST (21 ºC) during the month that the maximum SST has been recorded. This minimum SST has been used as indicator to compare different datasets. Orange lines is 25 ºC isotherm used to estimate the maximum extension of upwelling. Positive SST gradients show upwelling while negative values indicate non-upwelling.

https://doi.org/10.5194/egusphere-2024-4175
Preprint. Discussion started: 27 January 2025

The comparative analysis between different wind stress (Fig. 2) and SST (Fig. 3) data shows that the best representation of wind-induced upwelling is provided by GLORYS (Fig. 2c, f) compared to ORAS5 (Fig. 2a, d) and ERA5 products (Fig. 2b, e). The good SST index is obtained with OSTIA (Fig. 3c, h). The poor representation of the SST index was observed with HadISST (Fig. 3d, i). This difference can be explained by the different spatial resolution (see Table). The GLORYS and OSTIA data have a higher resolution to represent the coastal upwelling processes than the ORAS5, ERA5 and HadISST products. The zonal Ekman transport and the wind stress curl-driven were underestimated in ERA5 compared to ORAS5 and GLORYS (Fig. 2a, c). The maximum magnitude (1.5 m2 s-1) observed in the atmospheric reanalysis is lower than that observed in the ocean reanalysis (≥2.5 m2 s-1). The TUM observed in different sections shows that the coastal upwelling is longer and stronger in the northern part (TMU of SST index ≥ 1000 ºC) than in the southern part (TMU of SST index ≤ 1000 ºC) of the upwelling region.

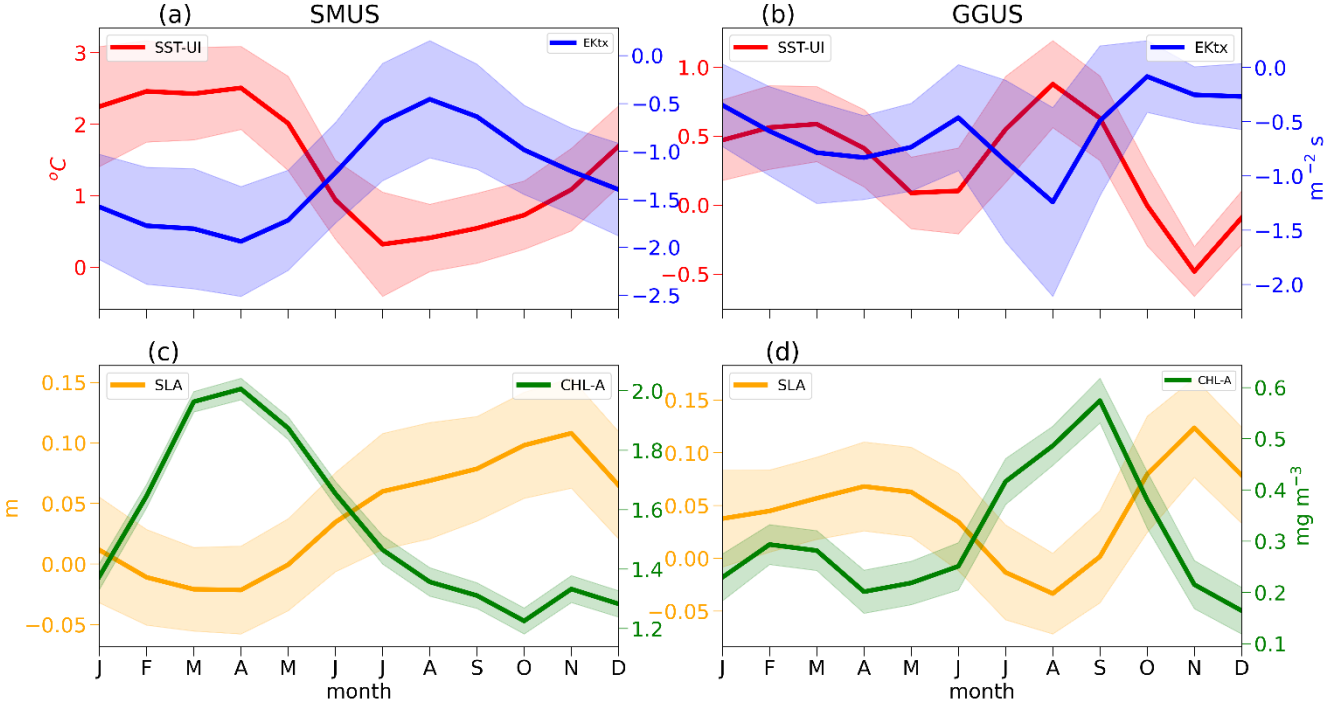

Figure 4: Annual cycle of upwelling indices in the Northwest African upwelling systems: a-b Ekman transport in (blue) and SST gradient (red) in the SMUS and GGUS, respectively. c-d Chlorophyll-a concentration (green) and sea level anomaly (orange) in both upwelling regions. The solid lines represent the climatological means while colour shadings are mean minus or plus standard deviation, and indicate the variability of each upwelling index.

The contribution of wind stress curl driven (WSCD), sea level anomaly (SLA), ocean current, and geostrophic balance were examined as additional upwelling indicators. Wind stress curl and geostrophic flow play an important role in modulating

https://doi.org/10.5194/egusphere-2024-4175
Preprint. Discussion started: 27 January 2025

coastal upwelling. The sign of these two indicators can indeed influence the dynamics of coastal upwelling. Negative geostrophic flows and positive WSCD generally enhance upwelling, while positive geostrophic flows and negative WSCD may reduce or suppress coastal upwelling. The result of Fig. 2d-f (contours) and Fig. 5a-b (colours) shows that of the WSCD and the ocean surface velocity strongly contribute to the enhancement of upwelling in the northern part of the SMUS, where the alongshore wind forcing persists over the years. In the south, where the alongshore wind forcing is seasonal, the Ekman

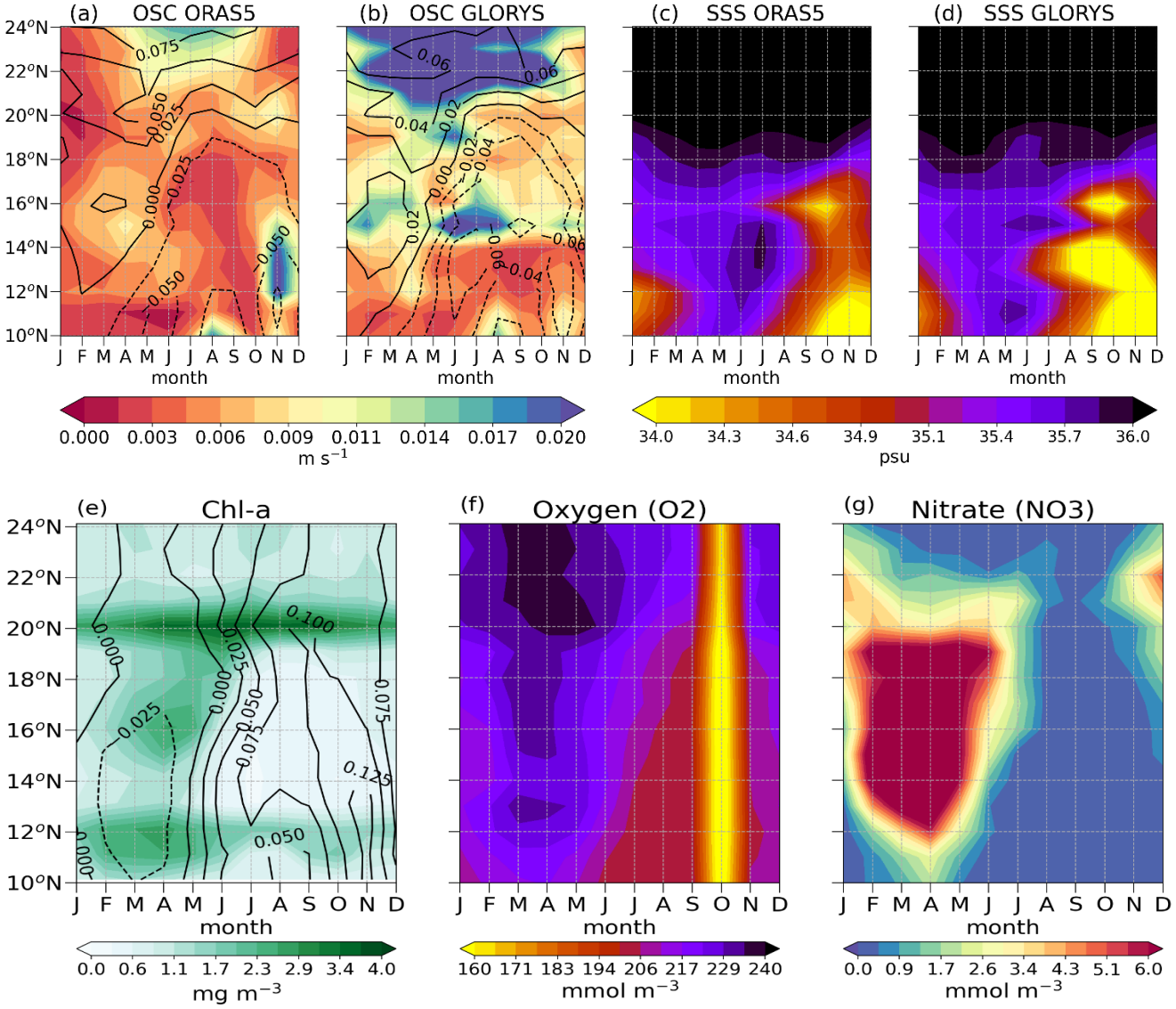

Figure 5: a, b Annual cycles of ocean surface velocity (colours) and geostrophic balance (contours) ORAS5 from ORAS5 and Global Ocean reanalysis (GLORYS). c, d Annual cycle of sea surface salinity from ORAS5 and GLORYS. e-g show Chlorophyll-a concentration, dissolved oxygen and nitrate in the Senegal-Mauritania upwelling system.

https://doi.org/10.5194/egusphere-2024-4175
Preprint. Discussion started: 27 January 2025

transport and the WSCD are statistically anti-correlated. The enhancement of upwelling is more related to the influence of the geostrophic balance (Fig. 5a-b), as the pressure gradient force is balanced by the Coriolis force. The Rossby circulation can modulate this upwelling by changing the geostrophic flow patterns. In the comparative analysis, the highest ocean surface velocity was observed with the GLORYS products (Fig. 5a) due to their high resolution compared to the reanalysis data (Fig. 5b).

The analysis of the SLA (Fig. 4) shows that the minimum peak of the SLA correlates well with the maxima peaks of the zonal Ekman transport, the coastal SST gradient (Fig. 4a) and the chlorophyll-a concentration (Fig. 4b) observed in April. However, the minimum peaks of the four upwelling indices show some delay. The minimum Ekman was observed in August, one month after the minimum peak of the SST gradient (Fig. 4a). In contrast, the minimum chlorophyll-a concentration is observed in October, one month before the maximum SLA (Fig. 4c). This minimum peak coincides with the maximum SST recorded in this region. The chlorophyll-a concentration reaches its maximum when the SLA is negative (Fig. 4c). This indicates that changes in SLA can influence the productivity of coastal upwelling.

Analysis of the annual cycles of sea surface salinity, dissolved oxygen and nitrate (Fig. 5c, d, f, g) shows that the maxima peaks of dissolved oxygen, nitrate and chlorophyll-a concentration (Fig. 5e) are driven by the maximum intensity of upwelling (April). However, the minimum peaks of these variables coincide with the highest SST (September-October). The highest values of dissolved oxygen and chlorophyll-a were found in the permanent upwelling region (above 21° N), while the maxima values of nitrate supply were observed in the seasonal upwelling region (below 21° N) during the upwelling season (December-June). The spatial distribution of sea surface salinity (Fig. 5c, d) also shows a strong difference between the north and the south. The maximum values (>35 psu) were observed in the permanent upwelling region, while lower values (≤35 psu) were observed in the southern part of the upwelling region.

3.1.2 Gulf of Guinea Upwelling System (GGUS)

In the GGUS, coastal upwelling indices were calculated with zonal wind stress and SST gradient. The upwelling waters were estimated under the 25° C SST isotherm. The annual cycle of the meridional Ekman transport shows two favourable upwelling periods (Fig. 6), as reported in previous studies (Addison, 2010; Sohou et al., 2020). A major summer upwelling period (July-September) and a minor winter upwelling period (February-March). However, the annual cycle of SST (Fig. 7) showed that the slight increase in meridional Ekman transport observed in winter was not strong enough to drive significant changes in local SST. The mean temperature was 27 °C, above the 25 °C threshold. The CUI obtained by integrating the meridional Ekman transport shows that the coastal upwelling starts in the 180th day of the Gregorian calendar (i.e., 68 days after the maximum downwelling in May) and continues for about 93 days before gradually decreasing until November. The maximum magnitude of the meridional Ekman transport (1.5 – 1.7 m2 s-1) and the SST gradient (0.8° - 1.4 °C) was observed in August when the

https://doi.org/10.5194/egusphere-2024-4175
Preprint. Discussion started: 27 January 2025

SST near the coast was around 23ºC. The cessation of upwelling activity was observed in September, one month after the maximum peak.

Analysis of the WSCD (Fig. 6, contours), the ocean velocity (colours) and the geostrophic balance (contours) (Fig. 8) shows that the intensity of the upwelling is influenced by the WSCD in the east (Fig. 6e-f) and by the ocean velocity and the vertical transport driven by the geostrophic balance (Fig. 8a, b) in the west of the upwelling region. This shows that a weakening of the meridional Ekman transport is often accompanied by an intensification of the WSCD upwelling (Bordbar et al., 2021). This result is more pronounced in the GLORYS than in the ORAS5 products.

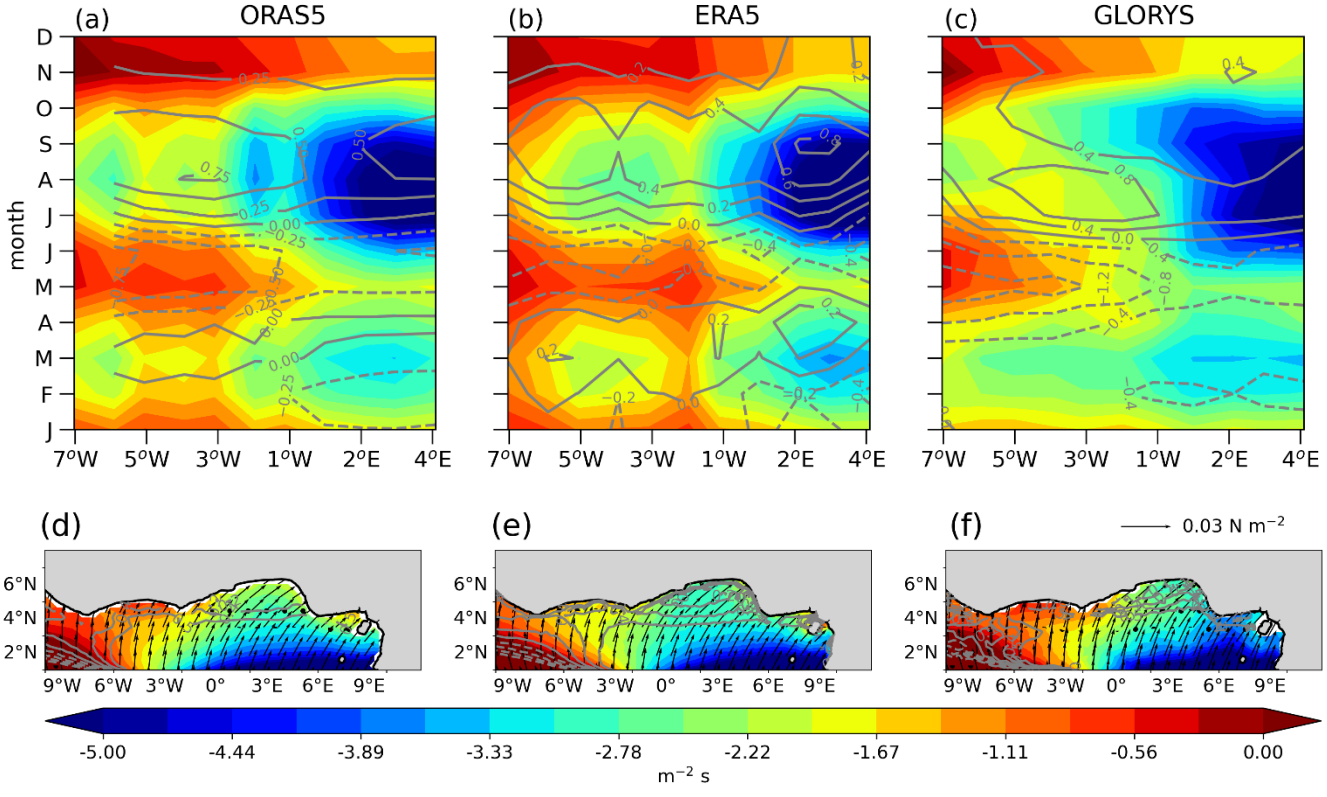

Figure 6: Wind stress driven-upwelling in the GGUS derived from ORAS5, ERA5 and GLORYS wind stress fields: a-c Annual cycles of the meridional Ekman transport (colours) and wind stress curl driven upwelling indices (contours). d-f Summer (from July to September: JAS) means of the wind stress (arrows) that drive the meridional Ekman transport, wind stress curl driven (contours) upwelling. Black dots represent the correlation coefficient (r>0.5) between zonal Ekman transport and SST gradient.

The obtained correlation coefficient between SST and meridional wind stress was statistically significant (r≥0.5) in the whole basin and does not allow to find the coherence between transport and coastal SST anomalies. As in the SMUS, the wind-driven upwelling index was underestimated in the ERA5 reanalysis (Fig. 6b, e) compared to the ocean reanalysis products (Fig. 7a, c, d, f). The strong SST gradient was observed in the OSTIA and GLORYS products (Fig. 7c, e) around 1.6 °C. The HadISST

https://doi.org/10.5194/egusphere-2024-4175
Preprint. Discussion started: 27 January 2025

still struggles to represent the coastal upwelling indices well (Fig. 7d) compared to reanalyses and satellite observations. The high meridional Ekman transport is observed with ORAS5 and ERA5 reanalyses (Fig. 6a, b) compared to GLORYS which shows a long duration of the upwelling season (Fig. 6c). The seasonal analysis of the SLA shows that the peaks of the SLA coincide with the SST gradient (Fig. 4c, d). The minimum SLA is observed with the maximum SST gradient, one month after the maximum peak of chlorophyll-a concentration. The maximum SLA was observed when the SST reached its minimum peak. This indicates the strong influence of the SLA on the coastal SST variability and upwelling productivity. The spatial analysis of the SST during the summer upwelling (Fig. 7) shows two upwelling cells: The western cell between 7º-1ºW and the eastern cell between 1ºW-4ºE. The meridional Ekman (Fig. 6) indicates that the wind-driven upwelling is stronger in the eastern cell, while the western cell is closely linked to the SLA (Illig et al. 2024) and ocean currents (Fig. 8a, b). This raises the idea of equatorial dynamics characterised by eastward propagation of Kelvin waves and trapped coastal waves (Philander et al., 1990; Clarke, 1983, Picaut, 1983; Polo et al., 2008) and ocean surface currents (Djakouré et al., 2017). In the western cell, the maxima of the SST gradient (≥0.8ºC) coincided with the minima of the SLA, whereas in the eastern cell (1ºW-4ºE), the maxima of the SST gradient (≤0.5ºC) are close to the peak of the meridional Ekman transport.

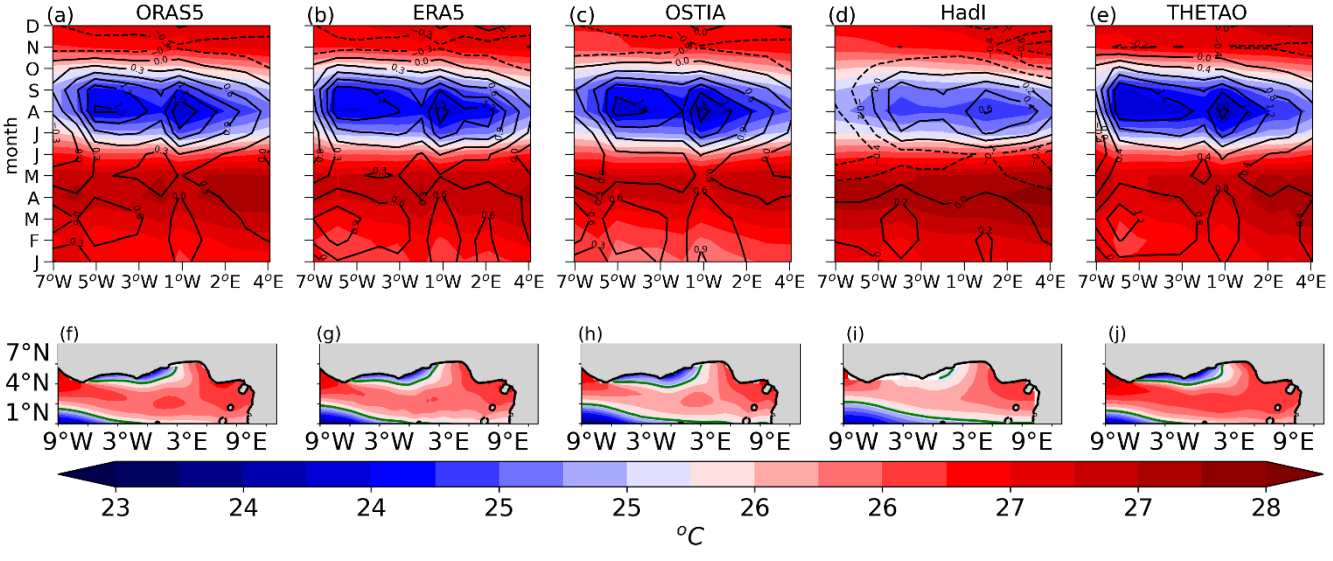

Figure 7: a-e Annual cycle of SST (colours) and upwelling indices (contours) in the GGUS. f-j Summer SST means (July-September). f-j Summer SST means. Green contours indicate the 25º C isotherm of SST used to define cold upwelled water.

The result of Fig. 8c-d shows that the maximum peaks of sea surface salinity (>34 psu) and nitrate are driven by intense upwelling events. The maximum concentration of chlorophyll-a concentration coincides with the maximum peak of dissolved oxygen (Fig. 8d, e). Maximum salinity (>34 psu) and nitrate are found during the upwelling period (Fig. 8c, d), with a maximum peak observed in the ORAS5 reanalysis (Fig. 8c). This difference between the datasets can be related to their

https://doi.org/10.5194/egusphere-2024-4175
Preprint. Discussion started: 27 January 2025

345 different spatial resolutions (Table). The seasonal analysis also showed that peaks in sea surface salinity and nitrate are driven by the intense upwelling events (August), while the maximum concentration of chlorophyll-a concentration is driven by the maximum peak of dissolved oxygen peak (Fig. 8d, e).

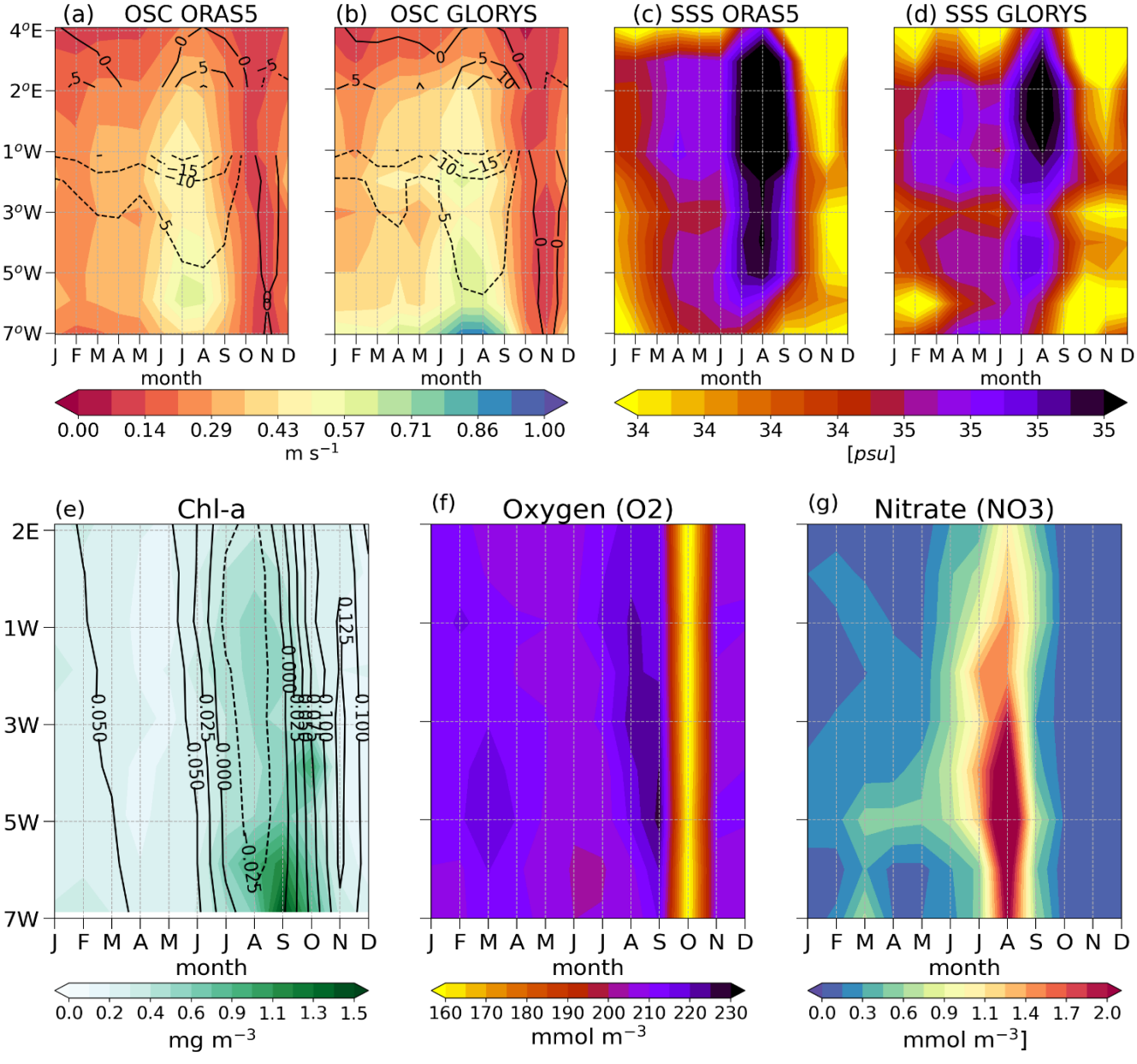

350

Figure 8: a, b Annual cycles of ocean surface velocity (colours) and geostrophic balance (contours) ORAS5 from ORAS5 and Global Ocean reanalysis (GLORYS). c, d Annual cycle of sea surface salinity from ORAS5 and GLORYS. e-g show Chlorophyll-a concentration, dissolved oxygen and nitrate in the Gulf of Guinea upwelling system.

https://doi.org/10.5194/egusphere-2024-4175
Preprint. Discussion started: 27 January 2025

4.2 Interannual variability and historical trends of Northwest African coastal upwelling

In the SMUS

This section analyses the year-to-year evolution of the upwelling indices. The interannual variability of the coastal upwelling indices in the SMUS was characterised by extreme surplus and deficit years. Years in which the value of the upwelling index was above the climatological mean plus the standard deviation were considered as surplus years, whereas the years in which the value of the upwelling index was below the climatological mean minus the standard deviation were considered as deficit years. The years between the climatological mean minus the standard deviation and the climatological mean plus the standard deviation were considered as normal upwelling years. Thus, the years 1984, 1989, 1990, 1993, 2008 and 2017 were characterised by an upwelling, while the years 1991, 2009 and 2022 were characterised by a deficit of the upwelling indices (Fig. 9). However, some years show deficits (1995, 2010) or surpluses (2000) of cold water amount north of 21ºN but not in the southern part of this latitude and vice versa. Analysis of Fig. 9 shows that the extreme years of wind-driven upwelling do not directly correspond to the extreme years of SST-based upwelling indices and vice versa. For example, 2008 and 2009 are surplus and deficit years respectively, for the amount of cold water driven by the zonal Ekman transport, but not for the SST gradient. Some of these extreme years have been observed in previous studies as ENSO years () and North Atlantic Niño or Niña years (Oettli et al., 2016; Lübbecke et al., 2019; Nnamchi et al., 2021). This has led us to investigate the link between the Northwest African coastal upwelling phenomena and the equatorial Pacific ENSO and North Atlantic Niño. Linear regression analysis of the upwelling indices shows a weak increasing trend of upwelling over the study period (slope=0.2). This increase was more slightly pronounced in the satellite observations than in the other data sets used. On the other hand, the reanalysis products show an almost constant variability of the upwelling (slope=0.01).

In the GGUS

The interannual analysis of upwelling indices in two sections of the GGUS (Fig. 10) highlights notable extreme years. Surplus upwelling indices were observed in 1983, 1998, 2010 and 2021, with a significant increase in upwelling compared to the climatological mean. Conversely, a slight deficit of coastal upwelling was observed in 1992, 2009 and 2015. However, the extreme years observed in the meridional Ekman transport differ from those found in the coastal SST anomalies. For example, 2021 was found to be the strongest wind-driven upwelling year during the study period, but was not driven by the strong cumulative SST gradient. In contrast, 2009, which was one of the deficit years of the meridional Ekman transport, was a strong year of the cumulative SST gradient. The analysis of the historical trends of the upwelling indices shows a decreasing trend of upwelling in the GGUS (slope=0.52). This decreasing trend can be linked to the anthropogenic climate change, which causes that warm water events such as marine heatwaves. As in the SMUS, most of the extreme years were observed as North Atlantic warm or cold years. This draws our attention to the relationship between equatorial variability modes and the GGUS upwelling.

https://doi.org/10.5194/egusphere-2024-4175
Preprint. Discussion started: 27 January 2025

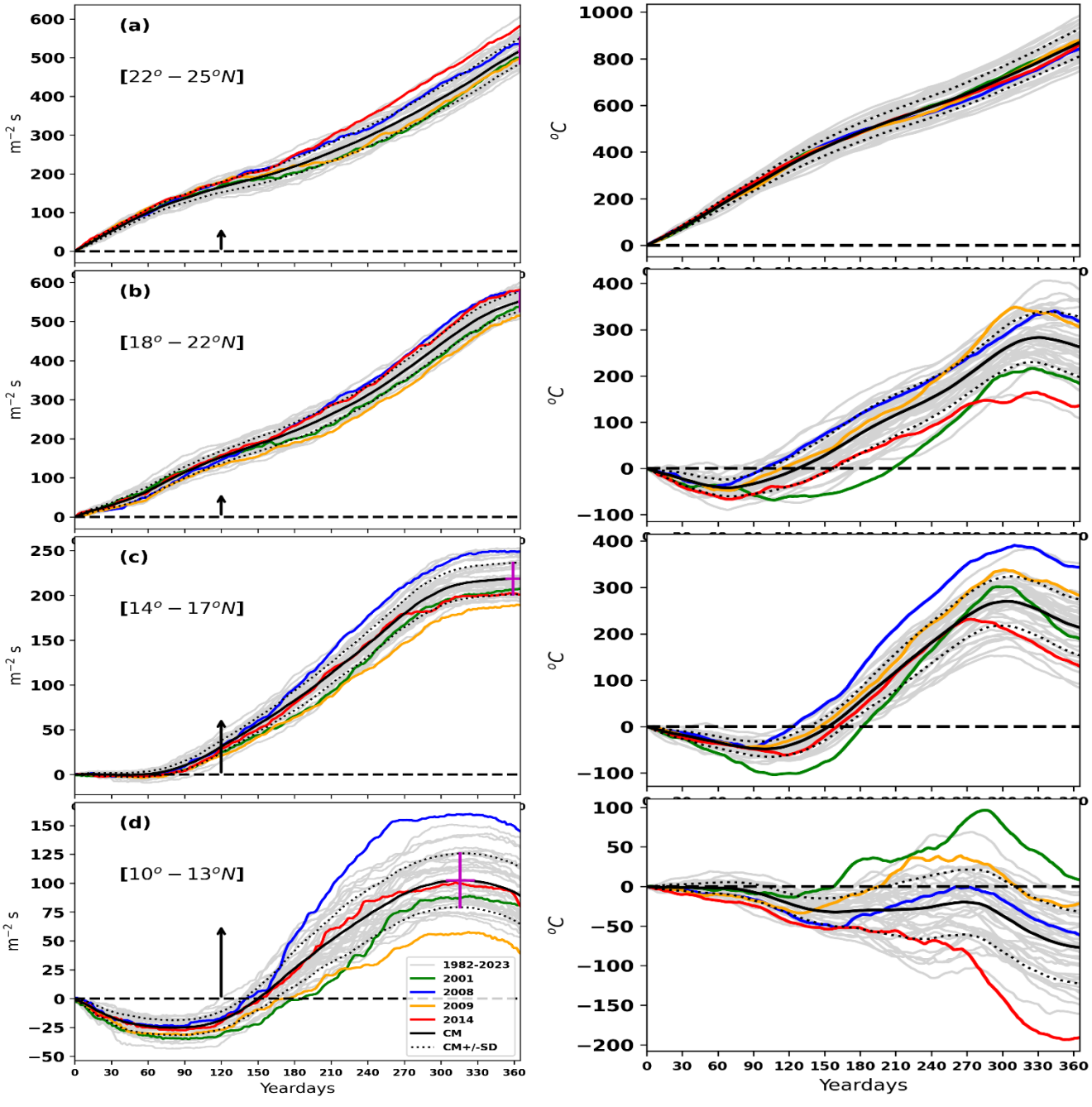

Figure 9: Interannual variability of upwelling in the SMUS: Cumulative upwelling index in four sections within the upwelling region. Grey curves indicate individual years from 1982 to 2022; solid black curves represent climatological means, while black dots show mean +/- standard deviation. Vertical red vector shows the onset of upwelling observed through the end of boreal Fall season (Fall starting index). Colours curves are extreme warm and cold years observed in this region.

https://doi.org/10.5194/egusphere-2024-4175
Preprint. Discussion started: 27 January 2025

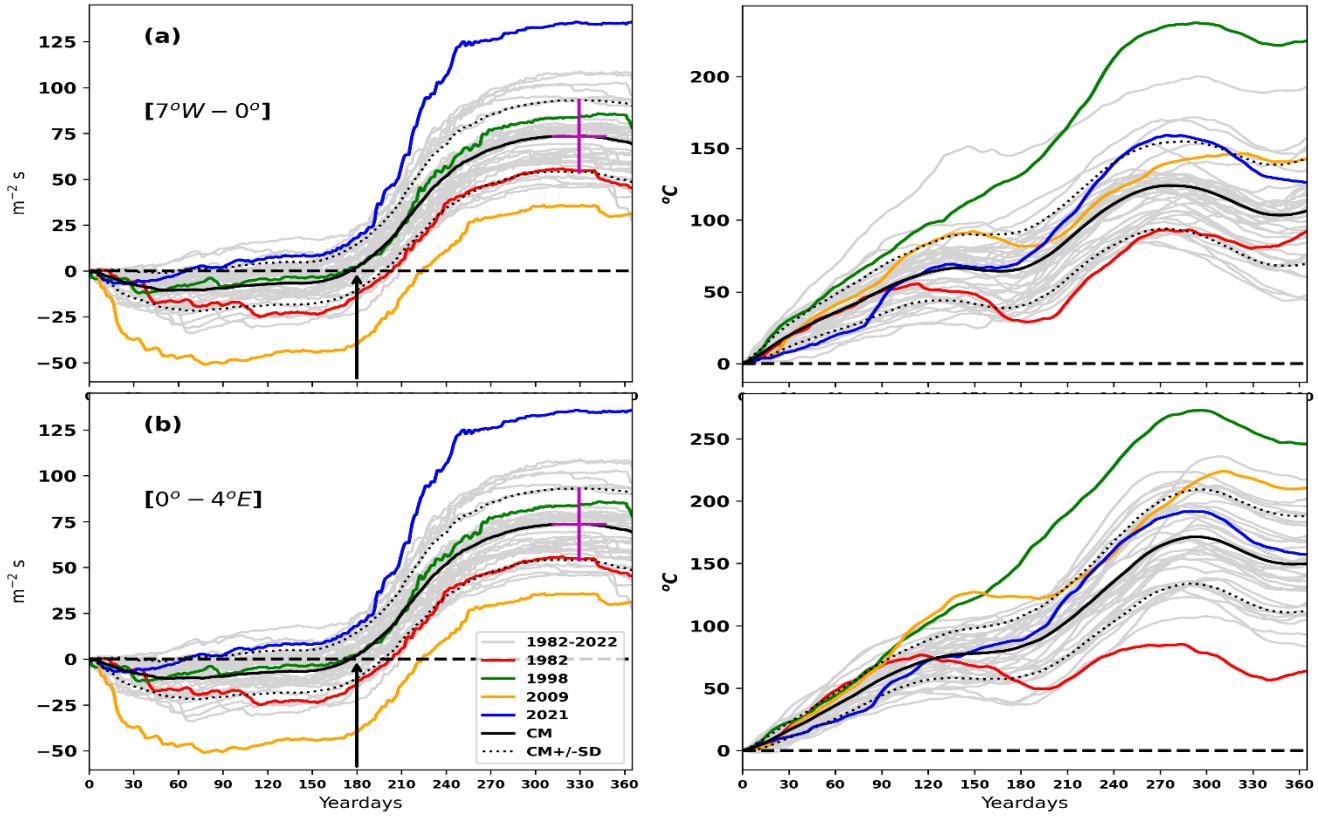

Figure 10: Interannual variability of upwelling in the GGUS: Cumulative upwelling index based on integrated zonal Ekman transport (a) and SST gradient (b). Grey curves indicate individual years from 1982 to 2022, solid black curves represent climatological means, while black dots show mean +/- standard deviation. Vertical red vector shows the onset of upwelling observed through the end of boreal spring season (spring start index). Colours curves are extreme warm and cold years observed in this region.

4.3 Connectivity between Northwest African coastal upwelling and Large-scale climate drivers

Previous studies have shown that changes in the intensity, frequency and duration can be influenced by large-scale climate drivers such as the Equatorial Pacific ENSO, NAO and PDO (Bograd et al., 2009, Lübbecke et al., 2019). In this section, the composite analysis of SST and wind stress anomalies for ten ENSO (Fig.11a-d) and North Atlantic Niño (Fig. 11e-f) years, shows a strong connection between ENSO events and SMUS. This connection is best developed during the boreal spring (Fig. 11c) following the most frequent season of maximum ENSO anomalies in the Pacific. The extreme Niño events drive extremely warm SST anomalies along the Senegal-Mauritania coasts, weakening the intensity and changing the direction of the coastal upwelling wind stress, but strengthening the cold-water flow in the Gulf of Guinea. This leads to significant changes in upwelling indices and metrics such as intensity, frequency and duration over the Northwest African coasts, especially in the SMUS. The link with El Niño is more obvious than with La Niña. Unlike the El Niño, the extreme events of La Nina enhanced

https://doi.org/10.5194/egusphere-2024-4175
Preprint. Discussion started: 27 January 2025

the upwelling current along the coasts of Senegal and Mauritania, but led to an accumulation of warm water in the Gulf of Guinea. As the Gulf of Guinea is close to the equator, the SST anomalies were more related to the equatorial Atlantic variability. The result of Fig 11e-d shows that the extremely warm SST events in the Equatorial Atlantic drive warm water along the Gulf of Guinea upwelling region, while the cold SST events drive cold water.

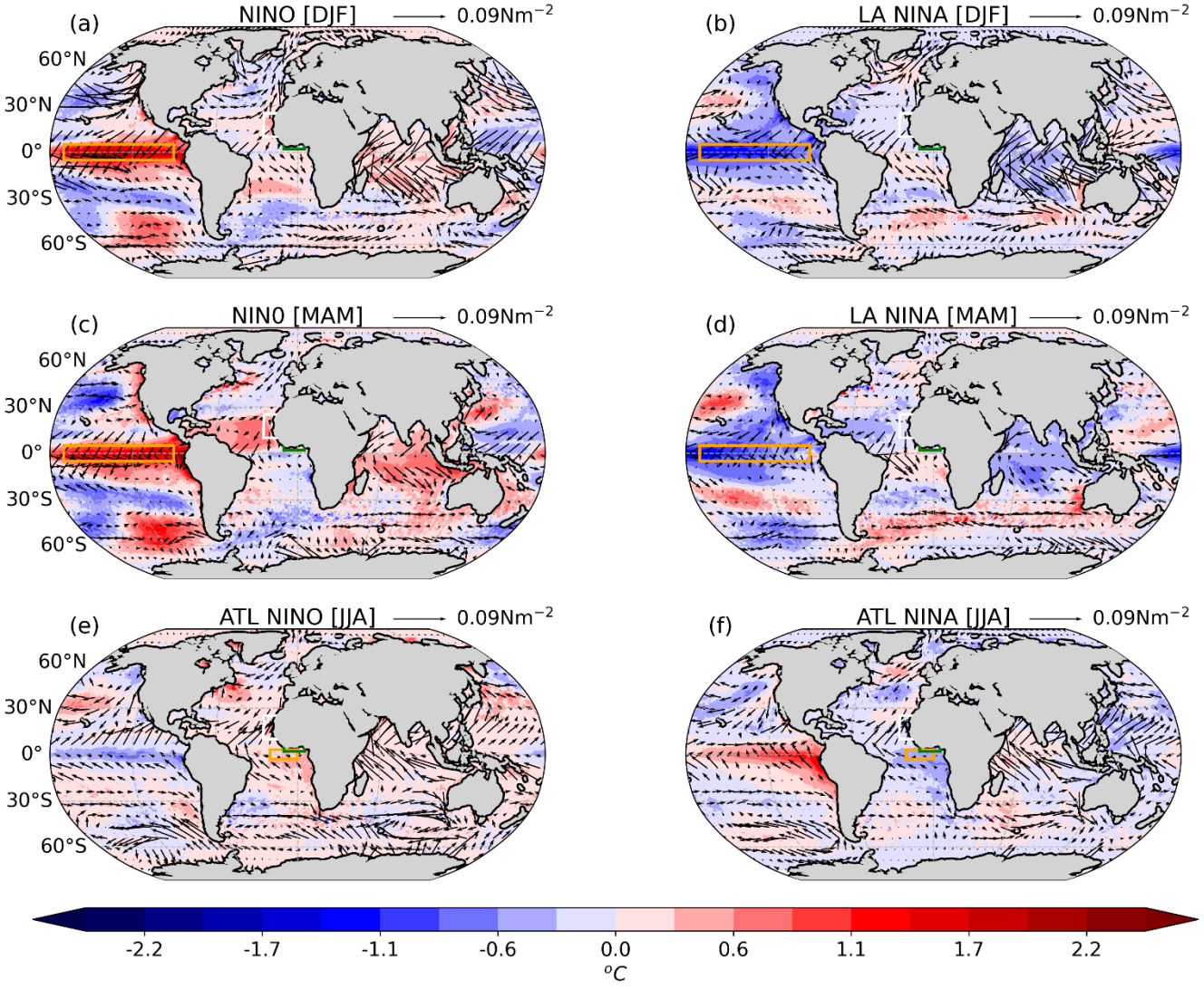

Figure. 11 Connection of ENSO and Atlantic variability to Northwest African upwelling systems. c-d Composite average of winter (December-February, DJF) and spring (March-April, MAM) extreme SST (colours) and wind stress (arrows) anomalies during extremes El Nino and La Nina years in the Equatorial Pacific. e-f Composite average of the summer (June-August, JJA) extreme SST (colours) and wind stress (arrows) anomalies during extreme warm and cold events in the Atlantic Niño region. Orange boxes show the ENSO area in the Equatorial Pacific (a-d) and Atlantic Niño (e-f) region. White and green boxes indicate the SMUS and GGUS, respectively.

https://doi.org/10.5194/egusphere-2024-4175
Preprint. Discussion started: 27 January 2025

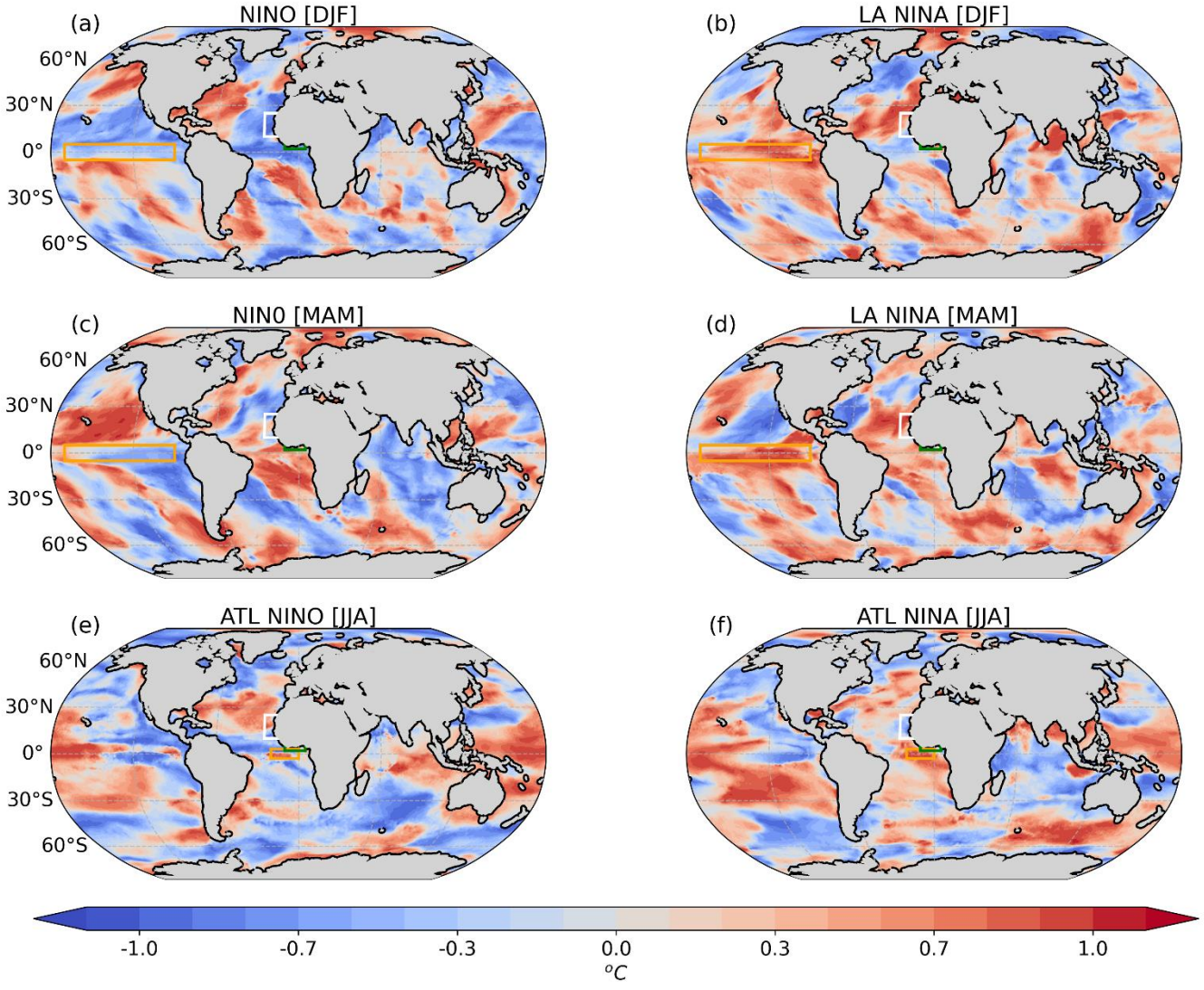

Figure 12: Composite correlation between upwelling favourable wind stress anomaly and equatorial variabilities during the extreme SST events: a-d Correlation coefficient between meridional wind stress and ENSO indices during winter (DJF) and spring (MAM) when the Senegal-Mauritania Upwelling reach its maximum peaks. e-f Correlation coefficient between zonal wind stress and Atlantic Niño indices. Orange boxes indicate equatorial Pacific ENSO (a-d) and Atlantic Nino (e-f) areas. White and green boxes show both Senegal-Mauritania and Gulf of Guinea upwelling systems.

A composite correlation between the Niño 3.4 index and upwelling-favourable wind stress anomalies (Fig. 12) provided more detail on the relationship between equatorial Pacific and Atlantic variability and the Northwest African coastal upwelling systems. A significant negative correlation (≥ -0.7) was observed between the Nino 3.4 index and meridional wind stress anomalies along the West African coasts during winter extreme Niño events (Fig. 12a). The same result was observed between

https://doi.org/10.5194/egusphere-2024-4175
Preprint. Discussion started: 27 January 2025

zonal wind stress and the Atlantic Nino index during the boreal summer in the GGUS and the southern part of the SMUS. This result shows that the intensification of El Niño was associated with a weakening of the upwelling wind stress accompanied by a significant reduction in the amount of upwelling water. In contrast, positive correlations were observed in boreal spring (MAM) during the extreme La Niña and Atlantic cooling events, respectively in the SMUS and GGUS (Fig. 12d, f). In summary, the results of the interaction between the North-West African coastal upwelling systems and the equatorial variability modes show that the interannual variability of the Senegal-Mauritania coastal upwelling is more related to ENSO events in the Pacific, whereas the interannual variability in the GGUS is more related to the equatorial Atlantic mode. However, in-depth studies are still needed to determine which drains the other.

Summary and discussion

Coastal upwelling in Northwest Africa was characterized using physical and biogeochemical marine variables from 1982 to 2022. The analysis was focused on the temporal and spatial variability of upwelling indices, analysing their seasonality and interannual variability during the boreal winter-spring and summer, when upwelling peaks in the Senegal-Mauritania (SMUS) and Gulf of Guinea (GGUS) regions, respectively. Upwelling trends were also examined by comparing different historical datasets. The variability of the upwelling indices was linked to large-scale climate drivers such as ENSO and Atlantic Niño events. In the SMUS (10-25ºN), the annual cycles of the upwelling indices showed a clear seasonal and latitudinal variability as observed in the previous studies (Benazouzz et al., 2014; Sylla et al., 2022). Cumulative upwelling indices derived from the daily SST and Ekman transport show that the onset of coastal upwelling is observed 120 days after the maximum downwelling in August and lasts about 245 to 270 days. Upwelling reaches its maximum intensity in April after 152 days of the onset, and then decrease progressively until August where minimm peaks of upwelling concide with the maximum downwelling. This variability in upwelling intensity was linked to fluctuations of the West African monsoon system and the Azores high pressure (Ndoye et al., 2014; Faye et al., 2015). The weakening of the coastal upwelling in the northern part of the SMUS was often accompanied by an intensification of the WSCD upwelling as observed in the Angola-Benguela upwelling system (Bordbar et al., 2021). The relatively weak correlation between Ekman transport and SST gradient observed in the south was previously explained by mesoscale eddy's activities and other environmental factors (Faye te al., 2015; Ndoye et al., 2017). A weak upwelling trend was observed during our study period. This historical trend was also observed in the whole Canary upwelling system (Ruela et al., 2020; Otero et al., 2023). Using climate model scenarios, previous studies (Sylla et al., 2019; Varela et al., 2022) found a continuous moderate increase of upwelling in the Canary upwelling system, in particular in the SMUS.
In the GGUS (7°W-4°E), the summer upwelling typically starts around the 180th day of the Gregorian calendar (i.e. 68 days after the maximum downwelling observed in May) and lasts for about 93 days. The SLA explain more of the SSTA variance for the GGUS system associated with clear upwelling characteristics in the western part (Sohou et al., 2020; Illig et al., 2024). The maximum SST fluctuations are around 0.8°C to 1.5°C in the west, while SSTAs remain weak in the eastern (less than 0.5°C). This indicates that coastal upwelling in the western of GGUS is more associated with coastal trapping driven by SLA

https://doi.org/10.5194/egusphere-2024-4175
Preprint. Discussion started: 27 January 2025

than coastal wind stress. The inverse situation is observed in the eastern part where coastal SSTAs is close with Ekman suctions (Ekman transport and WSCD). However, our results also showed that the variability of upwelling in the western part is also influenced by ocean surface currents. Using a regional ocean model, Djakouré et al., (2017) linked this coastal upwelling to the influence of Guinea Current. The influence of the vercal transport observed in the eastern part of the upwelling were recently highlighted by Brandt et al., (2023). These authors explained how vertical mixing can drive upwelling water at the surface. The interannual variability of the upwelling indices in both regions showed that coastal upwelling over the Northwest Coast is sensitive to equatorial Pacific ENSO events and Atlantic oscillations (NAO and Atlantic Niño). These climate drivers weaken wind stress and extremely warm SST events, which are likely to influence the timing, duration and intensity of upwelling events, sometimes leading to delays, early cessation or even suppression of upwelling (Bograd et al., 2009; Yu et al., 2020). In the SMUS, the extremely warm water event (El Niño) caused the winter upwelling indices to decrease, resulting in a weakening of the upwelling season. The opposite event (La Niña) caused a slight increase in upwelling. In addition, the upwelling indices based on SST anomalies sometimes deviated from the wind stress patterns. Analysis of historical trends indicated a moderate increase in upwelling intensity in the SMUS (Sylla et al., 2019) and a decrease in the GGUS that can be linked to anthropogenic climate change which drives extremely warm water events such as marine heatwaves. These results highlight the complex interplay between local upwelling dynamics and large-scale climate drivers, and emphasise the need for continued analysis to better understand and predict future changes in these vital coastal ecosystems.

Data availability: open-source datasets were used for this study. ORAS5 global ocean reanalysis monthly data used is available from 1958 to present, and freely downloadable from Copernicus Climate Change Service (C3S) Climate Data Store (CDS). DOI: 10.24381/cds.67e8eeb7 (Zuo et al., 2018). ERA5 data is available on the European Centre for Medium-Range Weather Forecasts (ECMWF) platform, 10.24381/cds.adbb2d47 (Hersbach et a., 2020)**.** The global Mercator Ocean reanalysis (GLORYS) products is open-source data available on Copernicus marine service server (https://marine.copernicus.eu) (Lellouche et al., 2021). Hadley Centre Sea Ice and SST dataset version 1 is available on through https://doi.org/10.1029/2002JD002670 (HadISST1; Rayner et al. 2003). The OSTIA-SST were accessed via the Copernicus Server (https://doi.org/10.48670/moi-00168, Good et al., 2020). The net chlorophyll-a concentration dataset used in this study covers from 1997 to 2023 and were derived from Copernicus Marine Environment Monitoring Service (CMEMS) (https://marine.copernicus.eu/). This dataset is provided by Moderate Resolution Imaging Spectroradiometer (MODIS) of the National Aeronautics and Space Administration (NASA). The bathymetry data used in this study are from the General Bathymetric Chart of the Oceans (GEBCO) 2023 grid, with a spatial resolution of 15 arc-seconds, freely available from https://www.gebco.net. Niño 3.4 indices were extracted from National Oceanic and Atmospheric Administration Climate Prediction Center plateform, https://www.cpc.ncep.noaa.gov/.

Authors' contributions: YD: Formal analysis and investigation, Writing-original draft preparation, visualization; IAB, BAS: supervision, management, resources, and conceptualization of the study. All authors contributed to the writing and revision of the manuscript.

https://doi.org/10.5194/egusphere-2024-4175
Preprint. Discussion started: 27 January 2025

Funding: This research was carried out as part of the West African Science Service Centre on Climate Change and Adapted Land Use (WASCAL) project, funded by the German Federal Ministry of Education and Research (BMBF).

Software: *Python (Version 3.11)* with Jupiter notebook computing environment was retrieved from https://www.python.org/

Competing interests*:* The authors declare no competing interests

Acknowledgements

This work used resources granted by West African Science Service Centre on Climate Change and Adapted Land Use (WASCAL). YD would like to thank the colleagues at Laboratory of Oceanography, Environmental and Climate Sciences (LOSEC), and at the Department of Physics at the University Assane Seck of Zinguichor (UASZ), Senegal, for the scientific discussions during his visit. We also thank the developers of Deepl and ChatGPT which is using this study for some grammatical and language correction.

References

Abrahams, A., Schlegel, R. W., and Smit, A. J.: Variation and change of upwelling dynamics detected in the world's eastern boundary upwelling systems, Frontiers in Marine Science, 8, 626411, 2021

Addison, N.: Investigation of the Upwelling Mechanism in the Gulf of Guinea. Master of Sciences report, CIPMA/UAC, Cotonou/Université de Toulouse III, 2010

Alory, G., Da-Allada, C. Y., Djakouré, S., Dadou, I., Jouanno, J., and Loemba, D. P.: Coastal upwelling limitation by onshore geostrophic flow in the Gulf of Guinea around the Niger River plume. Frontiers in Marine Science, 7, 607216. https://doi.org/10.3389/fmars.2020.607216, 2021

Alvarez, I., Lorenzo, M. N., DeCastro, M., and Gomez-Gesteira, M.: Coastal upwelling trends under future warming scenarios from the CORDEX project along the Galician coast (NW Iberian Peninsula). International Journal of Climatology, 37(8), 3427-3438. https://doi.org/10.1002/joc.4927, 2017

Amemou, H., Koné, V., Aman, A. and Lett, C.: Assessment of a Lagrangian model using trajectories of oceanographic drifters and fishing devices in the Tropical Atlantic Ocean. Progress in Oceanography, 188, 102426, 2020

Bakun, A.: Coastal upwelling indices, west coast of North America, 1946-71. NOAA Technical Report. https://repository.library.noaa.gov/view/noaa/9041/noaa_9041_DS1.pdf, 1973

Bakun, A.: Daily and weekly upwelling indices, west coast of North America, 1967-73 (Vol. 693). Department of Commerce, National Oceanic and Atmospheic Administration, National Marine Fisheries Service, 1975

Bakun, A.: Global climate change and intensification of coastal ocean upwelling. Science, 247(4939), 198-201. DOI: 10.1126/science.247.4939.198, 1990

Benazzouz, A., Pelegrí, J. L., Demarcq, H., Machín, F., Mason, E., Orbi, A., and Soumia, M.: On the temporal memory of coastal upwelling off NW Africa. Journal of Geophysical Research: Oceans, 119(9), 6356-6380. https://doi.org/10.1002/2013JC009559, 2014

https://doi.org/10.5194/egusphere-2024-4175
Preprint. Discussion started: 27 January 2025

Benazzouz, A., Demarcq, H., González-Nuevo, G., and de Vigo, C. O.: Recent changes and trends of the upwelling intensity in the Canary Current Large Marine Ecosystem. Oceanographic and biological features in the Canary Current Large Marine Ecosystem, 115, 321-330, 2015

Berraho, A., Somoue, L., Hernández-León, S., Valdés, L., & Valdés, L.: Zooplankton in the canary current large marine ecosystem, 2015

Binet, D., and Marchal, E.: The large marine ecosystem of shelf areas in the Gulf of Guinea: long-term variability induced by climatic changes. Large marine ecosystems: stress, mitigation, and sustainability, 104-118, 1993

Bordbar, M. H., Mohrholz, V., & Schmidt, M.: The relation of wind-driven coastal and offshore upwelling in the Benguela Upwelling System. Journal of Physical Oceanography, 51(10), 3117-3133. DOI: https://doi.org/10.1175/JPO-D-20-0297.1, 2021

Brandt, P., Caniaux, G., Bourles, B., Lazar, A., Dengler, M., Funk, A., and Marin, F.: Equatorial upper-ocean dynamics and their interaction with the West African monsoon. Atmospheric Science Letters, 12(1), 24-30, 2011

Brandt, P., Alory, G., Awo, F. M., Dengler, M., Djakouré, S., Imbol Koungue, R. A., and Rouault, M.: Physical processes and biological productivity in the upwelling regions of the tropical Atlantic. Ocean Science, 19(3), 581-601. https://doi.org/10.5194/os-19-581-2023, 2023

Bograd, S. J., Schroeder, I., Sarkar, N., Qiu, X., Sydeman, W. J., and Schwing, F. B.: Phenology of coastal upwelling in the California Current. Geophysical Research Letters, 36(1), 2009

Cabos Narvaez, W. D., Vázquez Medina, R., Parras Berrocal, I. M., Sein, D. V., Mañanes, R., and Izquierdo, A.: Assessment of the Canary current upwelling system in a regionally coupled climate model. https://doi.org/10.1007/s00382-021-05890-x, 2021

Chang, P., Xu, G., Kurian, J., Small, R. J., Danabasoglu, G., Yeager, S., and Chapman, P.: Uncertain future of sustainable fisheries environment in eastern boundary upwelling zones under climate change. Communications Earth & Environment, 4(1), 19, 2023

Caniaux, G., Giordani, H., Redelsperger, J. L., Guichard, F., Key, E., and Wade, M.: Coupling between the Atlantic cold tongue and the West African monsoon in boreal spring and summer. Journal of Geophysical Research: Oceans, 116(C4). https://doi.org/10.1029/2010JC006570, 2011

Clarke, A. J. and Battisti, D. S.: Identification of the fortnightly wave observed along the northern coast of the Gulf of Guinea. Journal of physical oceanography, 13(12), 2192-2200, 1983

Coëtlogon, G. D., Janicot, S., and Lazar, A.: Intraseasonal variability of the ocean—atmosphere coupling in the Gulf of Guinea during boreal spring and summer. Quarterly Journal of the Royal Meteorological Society, 136(S1), 426-441. https://doi.org/10.1002/qj.554, 2010

Coëtlogon, G., Deroubaix, A., Flamant, C., Menut, L., and Gaetani, M.: Impact of the Guinea coast upwelling on atmospheric dynamics, precipitation and pollutant transport over southern West Africa. Atmospheric Chemistry and Physics, 23(24), 15507-15521. https://doi.org/10.5194/acp-23-15507-2023, 2023

Cropper, T. E., Hanna, E., and Bigg, G. R.: Spatial and temporal seasonal trends in coastal upwelling off Northwest Africa, 1981–2012. Deep Sea Research Part I: Oceanographic Research Papers, 86, 94-111. https://doi.org/10.1016/j.dsr.2014.01.007, 2014

Demarcq, H., and Faure, V.: Coastal upwelling and associated retention indices derived from satellite SST. Application to Octopus vulgaris recruitment. Oceanologica acta, 23(4), 391-408. https://doi.org/10.1016/S0399-1784(00)01113-0, 2000

Djakouré, S., Penven, P., Bourlès, B., Veitch, J., and Koné, V.: Coastally trapped eddies in the north of the G ulf of G uinea. Journal of Geophysical Research: Oceans, 119(10), 6805-6819. https://doi.org/10.1002/2014JC010243, 2014

Djakouré, S., Penven, P., Bourlès, B., Koné, V., and Veitch, J.: Respective roles of the Guinea Current and local winds on the coastal upwelling in the northern Gulf of Guinea. *Journal of Physical Oceanography*, *47*(6), 1367-1387, 2017

https://doi.org/10.5194/egusphere-2024-4175
Preprint. Discussion started: 27 January 2025

Ekman, V. W.: On the Influence of Earth's Rotation on Ocean-Currents. Astromnomi O. Fysisk, 11, 51, 1905

Faye, S., Lazar, A., Sow, B. A., and Gaye, A. T.: A model study of the seasonality of sea surface temperature and circulation in the Atlantic North-eastern Tropical Upwelling System. Frontiers in Physics, 3, 76. https://doi.org/10.3389/fphy.2015.00076, 2015

Fontaine, B., & Janicot, S.: Wind-field coherence and its variations over West Africa. Journal of Climate, 512-524, 1992

Good, S., Fiedler, E., Mao, C., Martin, M. J., Maycock, A., Reid, R., and Worsfold, M.: The current configuration of the OSTIA system for operational production of foundation sea surface temperature and ice concentration analyses. Remote Sensing, 12(4), 720, 2020

Gruber, N.: Warming up, turning sour, losing breath: ocean biogeochemistry under global change. Philosophical Transactions of the Royal Society A: Mathematical, Physical and Engineering Sciences, 369(1943), 1980-1996, 2011

Hersbach, H., Bell, B., Berrisford, P., Hirahara, S., Horányi, A., and Muñoz-Sabater, J., The ERA5 global reanalysis. Q J R Meteorol Soc. 2020; 146: 1999–2049. https://doi.org/10.1002/qj.3803, 2020

Hormann, V., and Brandt, P.: Upper equatorial Atlantic variability during 2002 and 2005 associated with equatorial Kelvin waves. Journal of Geophysical Research: Oceans, 114(C3). https://doi.org/10.1029/2008JC005101, 2009

Illig, S., Djakouré, S., and Mitchodigni, T.: Influence of the remote equatorial dynamics on the interannual variability along the northern coast of the Gulf of Guinea. Journal of Geophysical Research: Oceans, 129(8), e2024JC021011, 2024

Koné, M., Djakouré, S., Adon, M., Ta, S., and Kouadio, Y.: Marine Heatwaves, Upwelling, and Atmospheric Conditions during the Monsoon Period at the Northern Coast of the Gulf of Guinea. Climate, 10(12), 199. https://doi.org/10.3390/cli10120199, 2022

Koné, V., Lett, C., Penven, P., Bourlès, B., and Djakouré, S.: A biophysical model of S. aurita early life history in the northern Gulf of Guinea. Progress in oceanography, 151, 83-96. https://doi.org/10.1016/j.pocean.2016.10.008, 2017

Körner, M., Brandt, P., Illig, S., Dengler, M., Subramaniam, A., Bachèlery, M. L., and Krahmann, G.: Coastal trapped waves and tidal mixing control primary production in the tropical Angolan upwelling system. Science Advances, 10(4), eadj6686. DOI: 10.1126/sciadv.adj6686, 2024

Lamb, P. J.: Large-scale tropical Atlantic surface circulation patterns associated with Subsaharan weather anomalies. Tellus, 30(3), 240-251, 1978

Ndoye, S., Capet, X., Estrade, P., Sow, B., Dagorne, D., Lazar, A., and Brehmer, P.: SST patterns and dynamics of the southern Senegal-Gambia upwelling center. Journal of Geophysical Research: Oceans, 119(12), 8315-8335. https://doi.org/10.1002/2014JC010242, 2014

Ndoye, S., Capet, X., Estrade, P., Sow, B., Machu, E., Brochier, T., ... & Brehmer, P.: Dynamics of a “low-enrichment high-retention” upwelling center over the southern Senegal shelf. Geophysical Research Letters, 44(10), 5034-5043. https://doi.org/10.1002/2017GL072789, 2017

Nnamchi, H. C., Latif, M., Keenlyside, N. S., Kjellsson, J., and Richter, I.: Diabatic heating governs the seasonality of the Atlantic Niño. Nature Communications, 12(1), 376, 2021

NOAA Climate Prediction Center.: Climate Indices: Monthly Atmospheric and Ocean Time Series. National Oceanic and Atmospheric Administration. Retrieved from https://www.cpc.ncep.noaa.gov/, 2023

Oettli, P., Morioka, Y., and Yamagata, T.: A regional climate mode discovered in the North Atlantic: Dakar Niño/Niña. Scientific Reports, 6(1), 18782. https://doi.org/10.1038/srep18782, 2016

Otero, P., Cabrero, Á., Alonso-Pérez, F., Gago, J., and Nogueira, E.: Temperature and salinity trends in the northern limit of the Canary Current Upwelling System. Science of The Total Environment, 901, 165791. https://doi.org/10.1016/j.scitotenv.2023.165791, 2023

https://doi.org/10.5194/egusphere-2024-4175
Preprint. Discussion started: 27 January 2025

Pardo, P. C., Padín, X. A., Gilcoto, M., Farina-Busto, L., and Pérez, F. F.: Evolution of upwelling systems coupled to the long-term variability in sea surface temperature and Ekman transport. Climate Research, 48(2-3), 231-246. https://doi.org/10.3354/cr00989, 2011

Pelegrí, J. L., Machín, F., and Hernández-Guerra, A.: Mass fluxes in the Canary Basin. *Progress in Oceanography*, *70*(2-4), 416-447, 2006

Pelegrí, J. L. and Peña-Izquierdo, J.: Eastern boundary currents off North-West Africa. IOC TECHNICAL SERIES, 115, 81-92. doi:URI: http://hdl.handle.net/1834/9179, 2015

Philander, S. G. H.: Upwelling in the Gulf of Guinea. Journal of Marine Research, 37, 23-33, 1979

Philander, S. G. H. and Pacanowski, R. C.: The oceanic response to cross-equatorial winds (with application to coastal upwelling in low latitudes). Tellus, 33, 201-210, 1981

Philander, S. G. H., Ravelo, A. C., Fairbanks, R. G.: Reconstructing tropical Atlantic hydrography using planktontic foraminifera and an ocean model. Paleoceanography, 5(3), 409-431, 1990

Picaut, J.: Propagation of the seasonal upwelling in the eastern equatorial Atlantic. Journal of Physical Oceanography, 13(1), 18-37, 1983

Polo, I., Lazar, A., Rodriguez-Fonseca, B., and Arnault, S.: Oceanic Kelvin waves and tropical Atlantic intraseasonal variability: 1. Kelvin wave characterization. Journal of Geophysical Research: Oceans, 113(C7), 2008

Rayner, N. A. A., Parker, D. E., Horton, E. B., Folland, C. K., Alexander, L. V., Rowell, D. P., and Kaplan, A.: Global analyses of sea surface temperature, sea ice, and night marine air temperature since the late nineteenth century. Journal of Geophysical Research: Atmospheres, 108(D14), 2003

Rodríguez-Fonseca, B., Mohino, E., Mechoso, C. R., Caminade, C., Biasutti, M., Gaetani, M., and Voldoire, A.: Variability and predictability of West African droughts: a review on the role of sea surface temperature anomalies. Journal of Climate, 28(10), 4034-4060, 2015

Roy, C. (1989). Fluctuations des vents et variabilité de l'upwelling devant les côtes de Sénégal. Oceanologica Acta, 12(4), 361-369., 1989

Sohou, Z., Koné, V., Da-Allada, Y. C., Djakouré, S., Bourlès, B., Racape, V., and Adje, C.: Seasonal and inter-annual ONSET Sea Surface Temperature variability along the northern coast of the Gulf of Guinea. Regional Studies in Marine Science, 35, 101129. https://doi.org/10.1016/j.rsma.2020.101129, 2020

Sydeman, W. J., García-Reyes, M., Schoeman, D. S., Rykaczewski, R. R., Thompson, S. A., Black, B. A., and Bograd, S. J.: Climate change and wind intensification in coastal upwelling ecosystems. Science, 345(6192), 77-80, 2014

Sylla, A., Mignot, J., Capet, X., and Gaye, A. T.: Weakening of the Senegalo–Mauritanian upwelling system under climate change. Climate Dynamics, 53, 4447-4473. https://doi.org/10.1007/s00382-019-04797-y, 2019

Sylla, A., Sanchez Gomez, E., Mignot, J., and López-Parages, J.: Impact of increased resolution on the representation of the Canary upwelling system in climate models. Geoscientific Model Development, 15(22), 8245-8267, 2022

Valdés, L., & Déniz-González, I.: Oceanographic and biological features in the Canary Current Large Marine Ecosystem, 2015

Varela, R., Rodríguez-Díaz, L., de Castro, M., and Gómez-Gesteira, M.: Influence of Canary upwelling system on coastal SST warming along the 21st century using CMIP6 GCMs. *Global and Planetary Change*, *208*, 103692, 2021

Varela, R., DeCastro, M., Rodriguez-Diaz, L., Dias, J. M., and Gómez-Gesteira, M.: Examining the ability of CMIP6 models to reproduce the upwelling SST imprint in the eastern boundary upwelling systems. Journal of Marine Science and Engineering, 10(12), 1970. https://doi.org/10.3390/jmse10121970, 2022

Vélez-Belchí, P., González-Carballo, M., Pérez-Hernández, M. D., and Hernández-Guerra, A.: Open ocean temperature and salinity trends in the Canary Current Large Marine Ecosystem. Centro Oceanográfico de Canarias, 2015

Weisberg, R. H., Horigan, A., and Colin, C.: Equatorially trapped Rossby-gravity wave propagation in the Gulf of Guinea. Journal of Marine Research, 37, 67-86, 1979

https://doi.org/10.5194/egusphere-2024-4175
Preprint. Discussion started: 27 January 2025

Yu, Y., Wang, Y., Cao, L., Tang, R., and Chai, F.: The ocean-atmosphere interaction over a summer upwelling system in the South China Sea. Journal of Marine Systems, 208, 103360, 2020

Zuo, H., Balmaseda, M. A., Mogensen, K., and Tietsche, S.: OCEAN5: The ECMWF Ocean reanalysis system and its real-time analysis component (p. 44). Reading, UK: European Centre for Medium-Range Weather Forecasts, 2018